Vol. 666: 31–55, 2021
https://doi.org/10.3354/meps13675

MARINE ECOLOGY PROGRESS SERIES
Mar Ecol Prog Ser

Published May 20

Arctic sea ice algae differ markedly from phytoplankton in their ecophysiological characteristics

Ane Cecilie Kvernvik[1,*], Clara Jule Marie Hoppe[2], Michael Greenacre[3], Sander Verbiest[4], Jozef Maria Wiktor[5], Tove M. Gabrielsen[1,6], Marit Reigstad[7], Eva Leu[8]

[1]The Department of Arctic Biology, University Centre in Svalbard, Svalbard Science Centre, 9171 Longyearbyen, Norway
[2]Marine Biogeoscience, Alfred Wegener Institut – Helmholtzzentrum für Polar- und Meeresforschung, 27570 Bremerhaven, Germany
[3]Department of Economics and Business, Universitat Pompeu Fabra and Barcelona Graduate School of Economics, Ramon Trias Fargas 25-27, 08005 Barcelona, Spain
[4]Department of Earth Sciences, Faculty of Geosciences, Utrecht University, Utrecht 3584 CB, The Netherlands
[5]Institute of Oceanology, Polish Academy of Sciences, 81-712 Sopot, Poland
[6]Centre for Coastal Research, University of Agder, 4604 Kristiansand, Norway
[7]Department of Arctic and Marine Biology, UiT The Arctic University of Norway, 9037 Tromsø, Norway
[8]Arctic R&D, Akvaplan-niva AS, Fram Centre, 9296 Tromsø, Norway

ABSTRACT: Photophysiological and biochemical characteristics were investigated in natural communities of Arctic sea ice algae and phytoplankton to understand their respective responses towards variable irradiance and nutrient regimes. This study revealed large differences in photosynthetic efficiency and capacity between the 2 types of algal assemblages. Sea ice algal assemblages clearly displayed increased photoprotective energy dissipation under the highest daily average irradiance levels (>8 µmol photons m^{-2} s^{-1}). In contrast, phytoplankton assemblages were generally light-limited within the same irradiance ranges. Furthermore, phytoplankton assemblages exhibited more efficient carbon assimilation rates in the low irradiance range compared to sea ice algae, possibly explaining the ability of phytoplankton to generate substantial under-ice blooms. They were also able to readily adjust and increase their carbon production to higher irradiances. The Arctic is warming more rapidly than any other oceanic region on the planet, and as a consequence, irradiance levels experienced by microalgae are expected to increase due to declining ice thickness and snow cover, as well as enhanced stratification. The results of this study suggest that sea ice algae may have less capacity to adapt to the expected environmental changes compared to phytoplankton. We therefore anticipate a change in sea ice-based vs. pelagic primary production with respect to timing and quantity in a future Arctic. The clearly distinct responses of sea ice algae vs. phytoplankton need to be incorporated into model scenarios of current and future Arctic algal blooms and considered when predicting implications for the entire ecosystem and associated biogeochemical fluxes.

KEY WORDS: Sea ice algae · Phytoplankton · Photoacclimation · Carbon fixation · Light · Nitrate · Primary production · Climate change

1. INTRODUCTION

In the ice-covered seas of the Arctic, 2 major functionally distinct types of primary producers are found: sea ice algae (i.e. living within or closely attached to sea ice), and phytoplankton (i.e. living in the water column, Leu et al. 2015). Sea ice algae are a key component of the Arctic food web, contributing up to 57% of total primary production in the central Arctic Ocean and between 3 and 25% in Arctic shelf

*Corresponding author: anek@unis.no

regions (Legendre et al. 1992, Gosselin et al. 1997, Arrigo et al. 2010, Loose et al. 2011). Sea ice algal production typically peaks in early spring when phytoplankton production is thought to still be very low, extending the total period of primary production in spring (Cota et al. 1991, Legendre et al. 1992). Furthermore, many Arctic marine organisms have adapted their life cycles to take advantage of this high-quality food source prior to the phytoplankton bloom (Runge et al. 1991, Søreide et al. 2006, 2010, Daase et al. 2013). Growth and succession in both sea ice and phytoplankton communities are controlled by several environmental variables, most importantly irradiance and nutrient availability (Tremblay & Gagnon 2009, Arrigo et al. 2014, Lewis et al. 2019), but also other drivers such as temperature and salinity (Coello-Camba et al. 2015, Torstensson et al. 2015). These physical factors vary greatly over time and space, and strongly influence physiology, abundance, biomass and taxonomic composition of differently adapted algal communities (Sakshaug 2004, Litchman & Klausmeier 2008).

Due to the contrasting physico-chemical environments in sea ice and open water, sea ice algae and phytoplankton exhibit specific adaptations to their respective habitats (Poulin et al. 2011, Kvernvik et al. 2020). Irradiance reaching the bottom of sea ice is principally regulated by ice thickness and overlaying snow cover, where the latter is usually most important due to its high light-attenuation properties (Gosselin et al. 1990, Mundy et al. 2005, Marks & King 2014, Hancke et al. 2018). As a result, reported transmittance through ice and snow layers in the Arctic is often very low (between 0.023 and 9% of incident irradiance; Leu et al. 2010, 2015, Campbell et al. 2016, Assmy et al. 2017, Hancke et al. 2018). Since sea ice algae live in a spatially restricted environment that is normally not undergoing rapid change, they usually experience rather gradually changing irradiances of low amplitudes (i.e. gradual changes in the sun's elevation, snow cover overlaid by diurnal fluctuation and variations in cloud cover). Concomitantly, sea ice algal communities are facing quite challenging growth conditions, such as sub-zero temperatures, high salinities and rapidly depleted nutrient and dissolved inorganic carbon (DIC) levels due to limited resupply and locally high densities of algal cells (Weeks & Ackley 1986, McMinn et al. 2014, Hill et al. 2018). In comparison, vertical mixing of phytoplankton cells within varying mixed surface layers implies strong and rapid fluctuations in light and sometimes nutrient regimes (MacIntyre et al. 2000), while salinity and DIC availability remain relatively stable. Phytoplankton species occurring in this environment can therefore be expected to cope better with dynamic light conditions.

Microalgae have evolved several mechanisms that allow them to acclimate to changes in irradiance, described as photoprotection and photoacclimation. The most important short-term (seconds to hours) photoprotective mechanisms involve increased non-photochemical quenching (NPQ) of excitation energy, which in diatoms is mainly driven by the de-epoxidation of xanthophyll cycling (e.g. diadinoxanthin and diatoxanthin; Lacour et al. 2020). On longer time scales (hours to days), microalgae can alter cellular pigment composition, e.g. by increasing antioxidant carotenes and xanthophylls as well as by decreasing the light-harvesting pigments in response to high irradiance (Brunet et al. 2011). Despite the ability of microalgae to acclimate to increasing irradiance, high light levels at potentially species-specific thresholds can still have negative physiological effects resulting in high light stress and photoinhibition (Barlow et al. 1988, Galindo et al. 2017). This can be a result of cells mostly acclimating to their average experienced growth environment, which is substantially lower than the experienced peak values (Behrenfeld et al. 1998, Van De Poll et al. 2005). Furthermore, photoacclimation by adjusting pigmentation takes more time (hours to days), hence, responding to rapidly increasing irradiance may remain a challenge for some algae at shorter time scales (Leu et al. 2006, Kvernvik et al. 2020).

Seasonally ice-covered seas at high latitudes are characterized by very pronounced algal spring blooms, usually starting with a sea ice bloom followed by a phytoplankton bloom. During the early stages when nutrients are plentiful, microalgal growth is often primarily limited by light (Leu et al. 2015). Later, because of intense algal growth during bloom events, inorganic nutrients become gradually depleted, and turn into a limiting factor for further biomass accumulation (Hansell et al. 1993, Varela et al. 2013, Danielson et al. 2017). In coastal Arctic regions, nitrogen is the main limiting nutrient (Strom et al. 2006, Van De Poll et al. 2016), which is often reflected in high carbon to nitrogen (C:N) ratios in microalgae (Niemi & Michel 2015). Nitrogen starvation may have considerable effects on microalgal photophysiology, because synthesizing proteins for photo-repair (such as D1 in the photosynthetic reaction center and Rubisco) and pigments for photoacclimation require high nutrient levels (Geider et al. 1993, Eberhard et al. 2008). Moreover, under nutrient limitation, a larger proportion of energy derived

from light reactions may be used for nutrient uptake rather than carbon fixation (Kulk et al. 2018). Hence, NO_3^- limitation can impede photoacclimation responses and increase the susceptibility to photoinhibition at high irradiance (Lewis et al. 2019). This is critical, since during the period of nutrient depletion, algal communities might also be exposed to high levels of irradiance as snow and ice melt (Nicolaus et al. 2012).

The Arctic is warming more rapidly than any other oceanic region on the planet, leading to a reduction in sea ice extent and thickness (Kwok et al. 2009, Screen et al. 2011), earlier sea ice melt onset (Nicolaus et al. 2012) and declining snow cover (Screen & Simmonds 2012), in addition to amplified river discharge due to increasing precipitation and terrestrial ice melt (Peterson et al. 2002). Since the underwater light climate in the high Arctic is primarily regulated by snow and ice cover (Mundy et al. 2005, Aumack & Juhl 2015), the Arctic Ocean is expected to shift from a predominantly light-controlled (ice-covered) to a more nutrient-controlled (open water) system (Carmack & Wassmann 2006). This may not only affect the physiological performance, but also competitiveness and biochemical characteristics of microalgae. Therefore, we expect major changes in microalgal community structure, succession and bloom phenology in the Arctic (Rat'kova & Wassmann 2002, Hegseth & Sundfjord 2008, Nöthig et al. 2015, Ardyna & Arrigo 2020), with potentially cascading effects at higher trophic levels. Sea ice and phytoplankton blooms do not only differ with respect to seasonal timing, but are also utilized by different groups of grazers, which will likely result in clearly distinct effects on higher trophic levels, when their relative contribution to Arctic primary production is altered (Søreide et al. 2010, Huntington et al. 2020). For developing realistic future scenarios, a proper mechanistic understanding of the physiological and biochemical responses of sea ice algae and phytoplankton towards their changing environment is essential. Of particular importance in this context is to understand how the balance between sea ice vs. phytoplankton primary production will change with respect to timing and quantity.

The aim of this study was to compare photophysiological and biochemical characteristics of natural sea ice algal vs. phytoplankton communities and identify their response to changes in the environment. To this end, we collected time series data of sea ice algae and phytoplankton from a high Arctic fjord, taking advantage of the rare co-occurrence of their respective spring blooms to conduct field experiments. We hypothesized that sea ice algae and phytoplankton display distinct differences in their responses towards changes in their abiotic environment, and expected sea ice algal communities to be less resistant towards high light stress compared to phytoplankton communities, as a result of their adaptation to 2 very different habitat types.

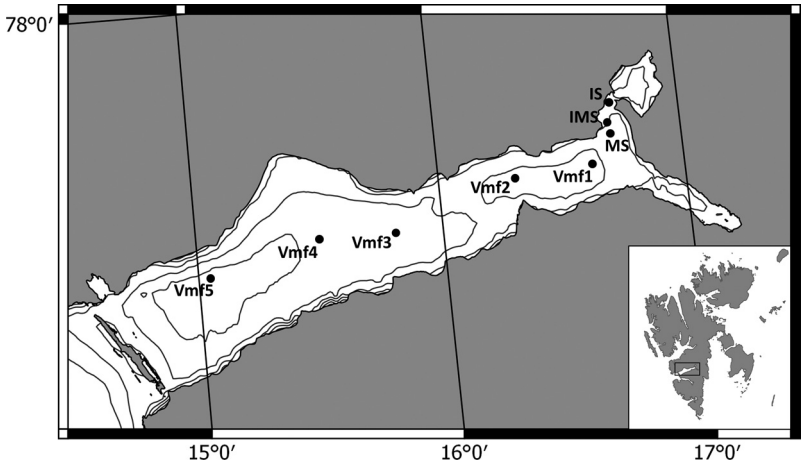

Fig. 1. Van Mijenfjorden, on the west coast of Spitsbergen (Svalbard, Norway), showing longitude, latitude and bathymetry (50 m resolution). Stations Vmf3 (bottom depth of 80 m), Vmf4 (88 m) and Vmf5 (116 m) are located in the outer basin, which is ~10 km wide and 100 m deep. The inner station (IS; 2 m), intermediate station (IMS; 14 m), main station (MS; 54 m), Vmf1 (78 m) and Vmf2 (61 m) are located in the inner basin, which is 5 km wide and has an average depth of ~30 m

2. MATERIALS AND METHODS

2.1. Study area

This study was conducted in Van Mijenfjorden, an approximately 10 km wide and 50 km long fjord located on the west coast of Spitsbergen, Norway (Fig. 1). The mouth of the fjord is largely closed off by the island Akseløya, which together with a shallow sill (<30 m) limits the exchange of fjord water with the warm and saline Atlantic water from the West Spitsbergen Current. Furthermore, the rather closed nature of the fjord leaves it less exposed to winds and waves, which offers favorable conditions for the formation of a stable sea ice cover. The fjord can be divided into an outer basin, which is ~10 km wide and 100 m deep, and an inner basin, which is 5 km wide and has an average

depth of ~30 m (Kangas 2000). Time for freeze-up usually covers a wide time span ranging from November to January, while the ice normally breaks up between June and July, depending on ice coverage and thickness (Høyland 2009).

2.2. Sample collection

Samples of sea ice algae and phytoplankton were collected from ice cores and in the water column from a total of 8 stations in Van Mijenfjorden between March and August 2017 (Fig. 1). Detailed information on stations, sampled depth, snow and ice thickness, irradiance, salinity, NO_3^- levels and temperature is provided in Table 1. Sea ice samples for community composition, elemental analysis and photosynthetic pigments were taken from the bottom 3 cm of sea ice cores collected using a Kovacs Mark2 core barrel (9 cm diameter; Kovacs Enterprise). On each sampling day, 3 sets of 6 cores each were taken approximately 1 m apart. To compare the effect of the different snow depths on sea ice algae, on 23 and 26 April and on 2 May, samples were taken from areas with low (0–5 cm) and high (20+ cm) snow cover. Snow depth and ice thickness for each core were recorded and averaged. Samples for filter-based bulk analyses were left for melting in darkness over 24 h (5–10°C), after adding 100 ml of GF/F filtrated seawater per cm of core to minimize osmotic stress (Bates & Cota 1986, Garrison & Buck 1986). After thawing, the volume of the samples was measured, and sets of 6 cores were pooled together in order to obtain 3 pools per station and per treatment in the case of low vs. high snow depth. From each pool, water was analyzed for community composition and filtered for pigment analysis (HPLC), particulate organic carbon and nitrogen (POC, PON) and chloro-

Table 1. Station names (see Fig. 1), sampling dates, sampled depths (phytoplankton only), snow and ice thickness, average daily irradiances, ocean/brine salinity, ocean/brine temperature, NO_3^- and chl *a* concentrations and the ratio of particulate organic carbon (POC):chl *a*. At each station, sea ice algae (S) and/or phytoplankton (P) were sampled. *Phytoplankton sampling conducted underneath the sea ice, while the rest was conducted in open water; na: not available

Stn	Sample	Date (d.mo.yr)	Depth (m)	Snow (cm)	Ice (cm)	Irradiance (µmol photons m^{-2} s^{-1})	Salinity (PSU)	Temp (°C)	NO_3^- (µmol l^{-1})	Chl *a* (µg l^{-1})	POC:chl *a* (µg C [µg chl *a*]$^{-1}$)
IS	S	28.04.17	na	7–8.5	57	5–6	33.9	−1.9	16.2	190.4	73.4
IM	S	28.04.17	na	19	55	3	28.7	−1.6	5.2	119.5	43.2
MS	S	09.03.17	na	8	29	2	35.6	−2.0	1.4	0.4	na
MS	S	07.04.17	na	4–8	49	3–9	28.7	−1.6	3.9	68.8	32.9
MS	S	23.04.17	na	3–3.5	55	20–22	33.9	−1.9	2.9	252.3	35.3
MS	S	23.04.17	na	19–20	55	4–5	35.1	−2.0	14.3	259.2	23.0
MS	S	02.05.17	na	0	52	74	31.6	−1.8	0.2	106.6	94.6
MS	S	02.05.17	na	20	52	7	31.4	−1.7	0.7	161.4	47.1
Vmf1	S	07.04.17	na	5–6	44	5–7	30.5	−1.7	12.4	300.7	20.4
Vmf1	S	30.04.17	na	15–16	40	10–11	29.8	−1.7	0.5	181.5	53.9
Vmf2	S	26.04.17	na	3.5–5	40	14–19	35.0	−2.0	0.8	72.5	57.5
Vmf2	S	26.04.17	na	26–27	40	3	33.4	−1.8	2.7	58.1	13.5
MS	P*	23.04.17	0	na	55	12	34.7	−1.8	9.6	0.4	945.3
MS	P*	02.05.17	0	na	52	40	34.6	−1.6	0.9	5.4	45.9
Vmf1	P*	30.04.17	0	na	40	11	34.6	−1.7	0.4	14.9	27.7
Vmf1	P	23.08.17	5	na	na	1	31.3	5.4	0.0	1.9	141.6
Vmf1	P	23.08.17	25	na	na	0	33.4	4.3	0.2	1.9	118.6
Vmf2	P*	26.04.17	0	na	40	10	34.6	−1.7	1.9	6.5	74.6
Vmf3	P	13.03.17	0	na	na	27	34.6	−1.4	10.2	0.1	na
Vmf3	P	13.03.17	5	na	na	13	34.6	−1.4	10.2	0.1	na
Vmf3	P	13.03.17	25	na	na	1	34.6	−1.4	9.6	0.1	na
Vmf4	P	13.06.17	5	na	na	63	34.3	1.8	1.2	0.5	657.3
Vmf4	P	13.06.17	25	na	na	1	34.5	0.5	1.5	0.6	428.4
Vmf4	P	13.06.17	50	na	na	0	34.5	0.1	1.6	0.4	691.2
Vmf4	P	23.08.17	5	na	na	20	31.9	5.5	0.0	2.5	100.6
Vmf4	P	23.08.17	25	na	na	0	33.5	4.6	0.0	4.8	42.1
Vmf5	P	14.03.17	0	na	na	33	34.5	−0.5	10.3	0.1	na
Vmf5	P	14.03.17	5	na	na	16	34.7	−0.7	10.2	0.1	na
Vmf5	P	14.03.17	25	na	na	1	34.7	−0.7	9.9	0.1	na

phyll (chl) *a* (see detailed description in Section 2.5). From each sampling event (date, station and low vs. high snow depth), 5 additional ice cores were taken: 3 for photophysiological measurements, 1 was left to thaw without the addition of filtered seawater, to be used for nutrient analysis, and 1 was used to measure ice temperature and left to thaw without addition of filtered seawater for salinity measurements (see detailed descriptions in Section 2.3). Phytoplankton sampling was performed using a 10 l Niskin bottle (Ocean Test Equipment) at different depths: 0, 5, 15, 25 and 50 m. Water from each depth was analyzed for community composition and filtered for pigment analysis (HPLC), particulate organic carbon and nitrogen (POC, PON) and chl *a* (see detailed description in Section 2.5). From each sampling event (date and station), additional Niskin bottles were taken at 0 m (ice-based sampling only), 5, 25 and 50 m for photophysiological measurements (see detailed description in Section 2.6).

2.3. Environmental parameters

Planar incoming and downwelling photosynthetically active radiation (PAR; 400–700 nm) was measured simultaneously at every sampling site and date between 11:00 and 13:00 h in Van Mijenfjorden, using 2 cosine-corrected 2π sensors (LI-192) coupled to a LI-1400 data logger (LI-COR). In this study, we wanted to identify responses of sea ice algae and phytoplankton towards changes in daily average irradiances, and hence calculated the daily incoming PAR (PAR_{24}) retrieved from LI-COR light sensors (Li-1800) monitoring PAR every 10 min in Adventdalen (~50 km north of Van Mijenfjorden). However, the cloud coverage was not always similar between the 2 fjords on the specific sampling days. Meteorological data comparing cloud coverage in addition to the incoming irradiance around noon in Van Mijenfjorden and Adventdalen were therefore used to choose the most similar days with respect to irradiance regimes between the 2 fjords (±1 d from the sampling date).

For the discrete PAR measurements at the ice–water interface in Van Mijenfjorden, 1 sensor was placed on the sea ice surface and the other sensor directly at the underside of the sea ice ~1.5 m south of the core hole using a folding L-shaped hinging arm. The incoming and transmitted planar downwelling PAR was used to calculate % transmitted irradiance through ice and snow depths (see Table S1 in the Supplement at www.int-res.com/articles/suppl/m666p031_supp.pdf). In order to calculate daily average irradiance at the ice–water interface (for sea ice algae), we multiplied the daily integrated PAR_{24} (see above) by the calculated % transmitted PAR for the specific station and date.

Similar measurements using the 2π PAR sensors (n = 2) and data logger were performed every meter (ranging from 0 to 40 m) for assessment of the light climate in open water, which were done from a small tender away from the larger main vessel, to reduce the shading effect of the vessel. The incoming and transmitted downwelling irradiances at 1 m depth were used to calculate % transmitted irradiance to surface waters, which was then multiplied by daily integrated PAR_{24} to estimate the daily irradiance in surface waters (E_0). The water column diffuse attenuation coefficient (K_d) was determined based on the Beer-Lambert law (Swinehart 1962). The daily irradiance at each sampling depth (E_Z) was calculated using the equation:

$$E_Z = E_0 \cdot \exp^{(-K_d \cdot Z)} \quad (1)$$

where E_0 is the daily surface irradiance (µmol photons m^{-2} s^{-1}), K_d is the diffuse light attenuation coefficient (m^{-1}), and Z is the sampling depth (m). For ice-covered stations, we used the calculated daily average irradiance at the ice–water interface as E_0.

In addition to the discrete light measurements during the sampling campaigns, we also collected continuous data of integrated PAR with loggers that were (1) mounted underneath the sea ice as part of a sea ice observatory close to Stn MS (see Fig. 1), and (2) part of an ocean observatory close to the position of Stn Vmf1, to compare temporal changes in the irradiance regimes at the ice–water interface and in open water. At the sea ice observatory, a LI-COR LI-192 Underwater Quantum Sensor was mounted 20 cm beneath the ice–water interface (ice thickness: 40 cm, snow depth: 3.5 cm at the time of deployment), measuring integrated PAR once per hour between 27 March and 2 May 2017. At the time of retrieval, the sea ice thickness above the sensor was ca. 30 cm and was covered by 27 cm of snow. Snow height was measured by a Snow Depth Buoy 2017S43 (Leu et al. 2018). The ocean observatory was deployed in late August 2016 at Stn Vmf1 and retrieved 1 yr later. An upward looking cosine-corrected Satlantic PAR sensor (model 1073) was placed at 12 m depth, and measured incoming irradiance every 2 h.

Ice temperatures were measured on every sampling date and station using a Testotherm 720 (Testo) thermometer inside small drill holes at 5 cm inter-

vals. Sea ice bulk salinity was measured on thawed sections of the core using a Symphony SP90M5 conductivity meter (VWR). Brine salinities were calculated from bulk salinity and ice temperature (Cox & Weeks 1986, Leppäranta & Manninen 1988). Water salinity (practical salinity unit, PSU) and temperature data (°C) were obtained from vertical CTD profiles (Mini STD model SD-204, SAIV). Nutrient samples were filtered using acid-washed syringes (10% HCl, 48 h) and GF/F filters (Whatman). Samples were stored at −20°C in 15 ml acid-washed Falcon tubes. After thawing, the samples were analyzed colorimetrically on a QuaAAtro autoanalyzer (Seal Analytical) using internal calibrations and CRMs (KANSO) for quality control. The samples were analyzed for PO_4^{3-} (limit of detection; 0.004 µmol l^{-1}), $Si(OH)_4$ (limit of detection; 0.01 µmol l^{-1}) and NO_3^- (limit of detection; 0.02 µmol l^{-1}) concentrations.

2.4. Species composition of algal communities

The species composition of sea ice and phytoplankton communities was analyzed to allow investigating of potential links between structural and ecophysiological characteristics. From each core section (sea ice algae) and water depth (phytoplankton), 250 ml samples were collected in brown bottles preserved with a glutaraldehyde-Lugol (35‰, v/v) solution (Rousseau et al. 1990). As sea ice algal samples had very high biomass, 0.5 ml of sample was suspended in 9.95 ml artificial seawater and left to settle in 10 ml Utermöhl chambers for 24 h (Utermöhl 1958). Phytoplankton samples were left to settle in 10 ml Utermöhl chambers for 24 h. Samples were analyzed for present and dominant species under an inverted microscope (Nikon TE-300) equipped with differential and phase contrasts. Samples were counted under 100 and 600× magnification and identified to the lowest taxonomic level possible.

2.5. Biochemical composition of algae

Samples for chl *a* determination were filtered (20–500 ml, depending on biomass) onto GF/F filters (Whatman) using a gentle vacuum, flash-frozen in liquid nitrogen and stored at −80°C until further analysis. Upon analysis, chl *a* filters were extracted in 10 ml methanol (≥99.9%) for 24 h at +4°C in the dark (Holm-Hansen & Riemann 1978) and measured on a 10-AU-005-CE Fluorometer (Turner Designs). POC/PON samples were filtered (50–600 ml, depending on biomass) onto pre-combusted (8 h, 450°C) GF/F filters and stored at −20°C in precombusted (12 h, 500°C) glass petri dishes. Prior to analysis, samples were acidified (0.2 ml of 0.2M HCl) and dried for 24 h. The samples were subsequently packed into tin capsules. Most samples were analyzed on a Euro EA 3000 elemental analyzer (Hekatech). Approximately one quarter of the samples were analyzed on a Flash EA 1112 elemental analyzer (Thermo Scientific) coupled to a Delta V Advantage IRMS (Thermo Scientific), since stable isotope ratios also needed to be determined for these samples (data not shown, published in Leu et al. 2020). For intercalibration of the different elemental analyzers, an acetanilide standard was used. C:N ratios were corrected based on the difference in atomic weight in carbon and nitrogen. Samples for pigment composition (100–300 ml) were collected when biomass was high (between 23 April and 2 May for sea ice algae and between 26 April and 23 August for phytoplankton; see Table 1 for sampling dates). Samples were filtered onto GF/F filters (Whatman), flash-frozen in liquid nitrogen and stored at −80°C until analysis. Frozen filters from algal cultures were extracted in a Teflon-lined screw-capped tube with 1.6 ml 95% methanol for 24 h, and then re-filtered through Millipore 0.45 µm filters, before the final extract was injected in the HPLC system. HPLC pigment analyses were performed as described by Rodriguez et al. (2006) using a Hewlett-Packard 1100 HPLC system with a quaternary pump and auto sampler. The identification of pigments was based on retention time and the optical density (OD) spectra of the pigment obtained with a diode array OD detector using pigment standards (Rodriguez et al. 2006).

2.6. Photophysiology by fast repetition rate (FRR) fluorometry

Chl *a* variable fluorescence was measured using a FastOcean FRR fluorometer (FFRf; Chelsea Technologies Group) in combination with an Act2 system (Chelsea). For sea ice algae, the bottommost 1 cm was quickly scraped off and kept in the dark until sufficient brine drainage was achieved (after ~5 min). Phytoplankton were sampled with Niskin bottles at different depths and put directly inside the Act2 chamber after sampling. Once placed inside the FRRf, cells were dark acclimated for >5 min, and subsequently exposed to a weak measuring light to record initial fluorescence (F_0). Thereafter, 120 single turnover (ST) saturation flashlets (blue LED color;

450 nm) with a duration of 2 µs were applied, to saturate PSII and determine maximal fluorescence (F_m) and the absorption cross section of PSII (σ_{PSII} [nm^2 $PSII^{-1}$]). ST saturation flashlets were followed by 60 relaxation flashlets, each with 40–60 µs duration, separated by 2.4 ms intervals, to record the rate of reopening of PSII reaction centers (τ_{ES} [ms]: Oxborough 2012). The maximum dark-acclimated quantum yield of PSII (F_v/F_m) was then calculated as $(F_m - F_0)/F_m$ (Krause & Weis 1991). To record fluorescence versus irradiance curves (fluorescence light curves, FLCs), the FastAct provided 10 × 3 min levels of white PAR (E_{PAR} [µmol photons m^{-2} s^{-1}]) ranging from 0 to 1500 µmol photons m^{-2} s^{-1}. Following actinic light periods, minimum (F'_0) and maximum (F'_m) fluorescence in light-exposed cells were determined. Relative electron transfer rates (rETRs [mol e^- (mol RCII)$^{-1}$ s^{-1}]) through PSII (Cosgrove & Borowitzka 2010) were calculated as:

$$\mathrm{rETR} = \frac{F'_m - F'_0}{F'_m} \cdot E_{PAR} \quad (2)$$

The calculated rETRs were plotted against actinic irradiance to generate FLCs, from which the light utilization coefficient (αETR [mol e^- m^2 (mol RCII)$^{-1}$ (mol photons)$^{-1}$]) and the maximum photosynthetic rate ($rETR_{max}$ [mol e^- (mol RCII)$^{-1}$ s^{-1}]) were derived using the model fit of Eilers & Peeters (1988). The photoacclimation index (E_kETR [µmol photons m^{-2} s^{-1}]) was then calculated as $rETR_{max}$/αETR. No spectral correction was applied to the data. NPQ of chl *a* fluorescence at irradiance of 300 µmol photons m^{-2} s^{-1} was calculated using the normalized Stern-Volmer coefficient, which treats the sum of non-photochemical processes present in a dark-acclimated sample (including non-radiative decay and fluorescence emission at F_m) as described by Oxborough (2012):

$$\mathrm{NPQ}_{300} = \frac{F'_0}{F'_m - F'_0} \quad (3)$$

where F'_0 and F'_m are the minimum and maximum fluorescence in cells exposed to 300 µmol photons m^{-2} s^{-1}, respectively.

2.7. *In situ* photosynthesis vs. irradiance incubation

Measurements of ^{14}C-based net primary production (NPP) *in situ* photosynthesis-irradiance curves were carried out between 1 and 2 May 2017 on samples of natural sea ice algal and phytoplankton assemblages moored for 24 h at the ice–water interface at Stn MS in Van Mijenfjorden (Fig. 1). Sea ice samples were collected from the bottom 1 cm of 3 thawed and pooled sea ice cores (snow depth: 8–9 cm), whereas phytoplankton samples were collected underneath the sea ice using 2 hauls of 20 µm phytoplankton nets between 0 and 5 m depth (KC; 24 cm diameter). The pooled samples were diluted with 700 ml GF/F filtered seawater and amended with 250 ml medium (20 ml of 50× concentrated f/2 medium [Sigma-Aldrich]; Guillard & Ryther 1962) mixed with 1 l of filtrated seawater) to prevent nutrient limitation during the incubation period. Final chl *a* concentrations were (mean ± SD) 71.1 ± 6.9 and 71.8 ± 7.7 µg l^{-1} for phytoplankton and sea ice algae, respectively. Triplicate samples of sea ice algae and phytoplankton were collected for chl *a* variable fluorescence measurements (FRRf) before the remaining samples were split into 20 ml subsamples (n = 12) and transferred to experimental bottles (50 ml capacity) with optical coating (transmission rates: 0–100%, Hydro-bios). For all NPP measurements, samples were amended with $NaH^{14}CO_3$ (PerkinElmer, 53.1 mCi $mmol^{-1}$ stock) giving a final ^{14}C specific activity of 1 µCi ml^{-1}. To determine the total activity in the incubations, 100 µl of radioactive sample were removed in duplicates and directly transferred to a clean scintillation vial containing 250 µl ethanolamine. Experimental bottles were then placed randomly on an incubation frame equipped with a PAR logger (DEFI 2-L sensor) measuring every 5 min and moored for 24 h underneath the sea ice (after snow was removed from the area). After incubation, samples were fixed with 2 drops of 37% formaldehyde before they were filtered onto GF/F-filters, acidified with 500 µl 1M HCl and left to degas overnight. Filters were then transferred into scintillation vials, and 6 h prior to analysis, 10 ml of scintillation cocktail (Ultima Gold AB, PerkinElmer) were added to the samples and total count vials. Subsequently, they were analyzed by means of a TriCarb 2900TR scintillation counter (PerkinElmer). ^{14}C fixation rates (µg C [µg chl *a*]$^{-1}$ d^{-1}) were calculated according to Hoppe et al. (2015). Calculated ^{14}C fixation rates were plotted against irradiance to generate photosynthesis versus irradiance (*PE*) curves, from which the initial light-limited slope of the *PE* curve (α [µg C (µg chl *a*)$^{-1}$ d^{-1} (µmol photons m^{-2} s^{-1})$^{-1}$]) and the maximum photosynthetic rate (P_{max} [µg C (µg chl *a*)$^{-1}$ d^{-1}]) were derived using the model fit of Eilers & Peeters (1988). The photoacclimation index (E_k [µmol photons m^{-2} s^{-1}]) was then calculated as P_{max}/α.

2.8. Statistical analysis

Student's *t*-tests with data following a normal distribution (Shapiro-Wilk test) were performed to evaluate significant differences between sea ice algae and phytoplankton of the photophysiological and biochemical parameters from field observations and the *in situ* incubation experiment (see Table 2 for parameters) using the program Sigmaplot (SysStat Software). Modeling of parameters as a function of irradiance and NO_3^- levels was performed with generalized additive mixed modeling (GAMM), using the 'gamm()' function in the R package 'mgcv' (Wood 2017, R Core Team 2017). Replicates for phytoplankton samples were modeled as being correlated if they were taken at the same station on the same day. For the sea ice samples, replicates were modeled as being correlated if they were taken at the same station on the same day and with the same snow cover, either low or high. All relationships were modeled as log–log ones, implying that the size effect is a percentage change in the response for a given percentage change in the predictor. In many cases, the GAMM diagnosed a linear relationship where the effect size was constant, but in a case where the relationship was nonlinear, the effect size changed depending on the predictor value. Relationships were plotted along with 95% confidence error curves, and when parameters were found to be significantly related to both irradiance and NO_3^-, contour plots were made using the function 'vis.gam(),' also in the 'mgcv' package. Effect sizes were deemed significant when the p-values were <0.05.

3. RESULTS

3.1. Environmental conditions

This study followed the development of sea ice algae from 9 March to 2 May 2017, and phytoplankton from 13 March to 28 August 2017 (Table 1). During the field campaign in Van Mijenfjorden in 2017, air temperature mainly remained below 0°C (ranging from −29 to 0°C) between early March and early May. After 31 May, air temperature consistently stayed above 0°C (Fig. 2a). Water temperatures at 12 m (retrieved from the multi-parameter ocean observatory) remained stable at ~1.8°C between early March and 30 April. Thereafter, water temperature started to increase gradually reaching temperatures >0°C by 13 June. By the end of the field campaign (28 August), the ocean temperature had increased to 5.4°C (Fig. 2a). Sea ice started to form in the inner basin at the end of January/early February and covered the fjord out to Stn Vmf4 by early May. The inner and outer basins were ice free from mid-June onwards (retrieved from http://polarview.met.no/). Ice thickness remained relatively stable between stations and sampling dates, ranging from 29 to 57 cm, while snow cover on sea ice was variable due to wind drift as well as melting processes later in the season, and ranged from 0 to 27 cm (Table 1). Temporal development of ice and snow thickness from early March to early May at Stn MS is shown in Fig. 2b.

The absolute range of daily average irradiance encountered by sampled sea ice algae was 2–74 µmol photons m^{-2} s^{-1}, with peak irradiance ranging from 12 to 305 µmol photons m^{-2} s^{-1}. PAR transmittance was highly variable due to changing snow cover, with 0.5% transmittance of incoming irradiance under the highest snow cover (27 cm) and 26% transmittance in areas without snow (Table S1). The absolute range of daily average irradiance encountered by phytoplankton was 0–63 µmol photons m^{-2} s^{-1} (Table 1), with peak irradiance ranging from 0 to 288 µmol photons m^{-2} s^{-1}. In March, daily surface irradiance in open water ranged from 27 (Vmf3) to 33 µmol photons m^{-2} s^{-1} (Vmf4), with peak irradiance of 192 and 267 µmol photons m^{-2} s^{-1}, respectively. In late April and early May, when phytoplankton sampling was conducted underneath sea ice, the daily irradiance levels at the ice–water interface ranged from 10 to 40 µmol photons m^{-2} s^{-1} (with peak irradiance from 24 to 26 µmol photons m^{-2} s^{-1}). During June and August, open water stations (Vmf1 and Vmf4) were influenced by meltwater and sediment loading from terrestrial runoff, leading to highly variable PAR levels, differing also between stations (Table 1). At Vmf4 in June, the daily average irradiance at 5 m depth was 63 µmol photons m^{-2} s^{-1} (with peak irradiance of 288 µmol photons m^{-2} s^{-1}), while in August the daily average irradiance at 5 m depth dropped to 20 µmol photons m^{-2} s^{-1} (with peak irradiance of 121 µmol photons m^{-2} s^{-1}). At Vmf1, the daily average irradiance was 1 µmol photons m^{-2} s^{-1} (with peak irradiance of 6 µmol photons m^{-2} s^{-1}) in August at 5 m depth. Both stations had very low irradiance levels at depths below 5 m in June and August (<1 µmol photons m^{-2} s^{-1}).

Regarding the temporal development of algal biomass, bottom sea ice chl *a* concentrations peaked in April with the highest concentrations found at Stn MS on 23 April (~270 µg l^{-1}), at Vmf1 on 8 April (~300 µg l^{-1}) and at Vmf2 on 26 April (~65 µg l^{-1}, Fig. 2c). In sea ice,

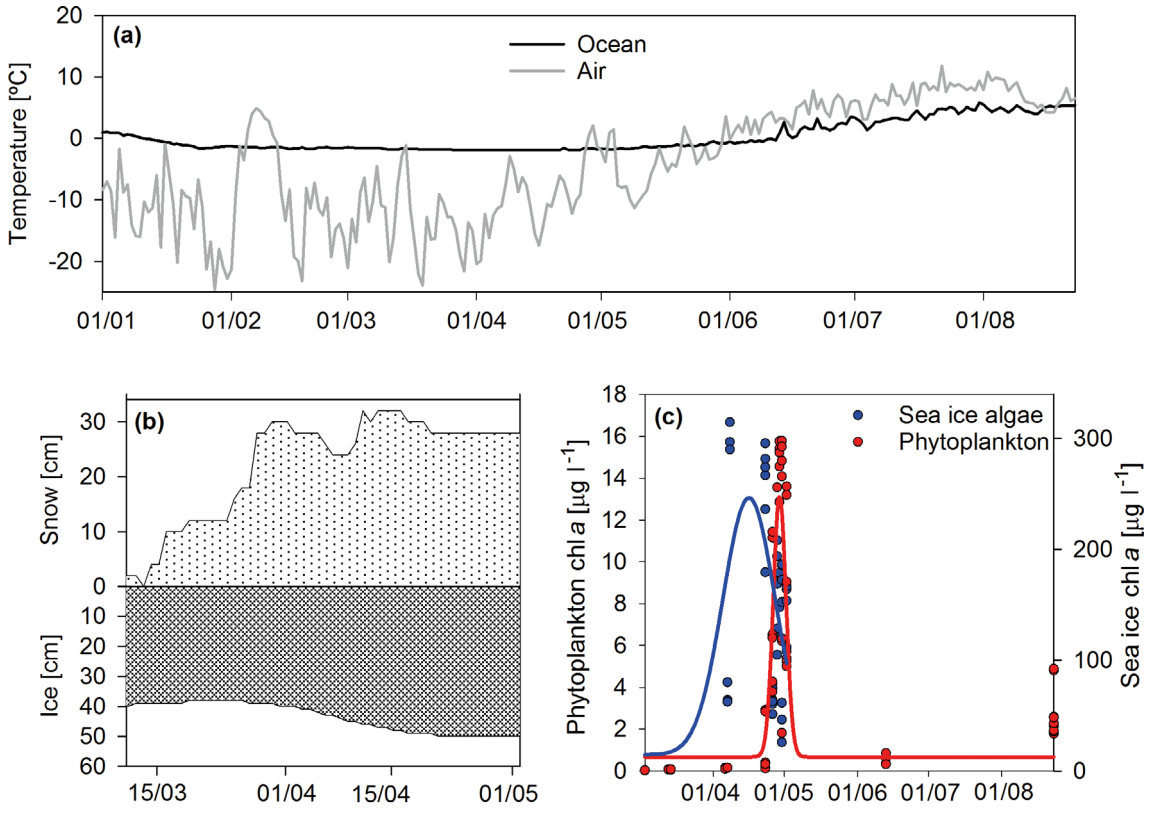

Fig. 2. Environmental conditions before and during the field campaign in Van Mijenfjorden in 2017 (dates given as d/mo). (a) Temporal development of ocean temperature (12 m depth at Vmf1, retrieved from the ocean observatory) and air temperature. (b) Temporal development of snow (cm) and ice (cm) thickness at the main station (MS, retrieved from the sea ice observatory). (c) Temporal development of sea ice algal and phytoplankton chl *a* concentrations during the field campaign. Data points in panel c represent single replicates from different sea ice cores (sea ice algae) and different depths (0–50 m: phytoplankton)

NO_3^- levels varied strongly between dates and stations, but dropped, on average, from (mean ± SD) 6.6 ± 5.3 in early March to 1.0 ± 0.9 µmol l^{-1} in early May (Table 1). Silicate and phosphate levels did not change significantly over time in sea ice, ranging from 1.09 ± 0.17 to 2.28 ± 0.21 µmol l^{-1}, respectively (data not shown, available in Hoppe et al. 2020). On 23 (at Stn MS) and 26 April (at Stn Vmf2) and on 2 May (at Stn MS), samples were taken from areas with low (0–5 cm) and high (20+ cm) snow cover. At all tested stations, NO_3^- levels were significantly lower under low compared to high snow cover (MS on 23 April: Student's *t*-test, $t_4 = 5.7$, p = 0.004); Vmf2 on 26 April: $t_4 = 14.3$, p = 0.0001; and Vmf2 on 2 May: $t_4 = 4.8$, p = 0.008). $Si(OH)_4$ and PO_4^{3-} concentrations remained statistically similar between low and high snow sites (data not shown, available in Hoppe et al. 2020). Brine temperature in the bottom 3 cm of the sea ice remained relative stable (ranging from –2.0 to –1.6°C), while brine salinity varied more, i.e. ranging from 28.7 to 35.6 (Table 1). Phytoplankton chl *a* concentrations approached ~16 µg l^{-1} between 23 April and 2 May (Fig. 2c). The accumulation of phytoplankton biomass resulted in a rapid drawdown of open water NO_3^- (from 9.9 ± 0.3 to 1.1 ± 0.6 µmol l^{-1}; Table 1) and $Si(OH)_4$ levels (from 4.4 ± 0.3 to 0.3 ± 0.2 µmol l^{-1}; data not shown, available in Hoppe et al. 2020) by the end of April. Phosphate concentrations decreased from an average of 0.46 ± 0.05 µmol l^{-1} in early March to 0.19 ± 0.09 µmol l^{-1} in August (data not shown, available in Hoppe et al. 2020). Water salinity remained fairly stable between stations and sampling dates during the field campaign (ranging from 31.2 to 34.6; Table 1).

3.2. Species composition of algal communities

Sea ice algal assemblages were mainly dominated by pennate diatoms (between 37 and 99% of total cell abundances) across all stations and throughout the sampling period (Fig. 3a). Particularly abundant taxa were *Nitzschia frigida*, *Navicula* sp. and *Fragilariopsis* sp. No coherent trends were observed when comparing sites with low and high snow depths. The

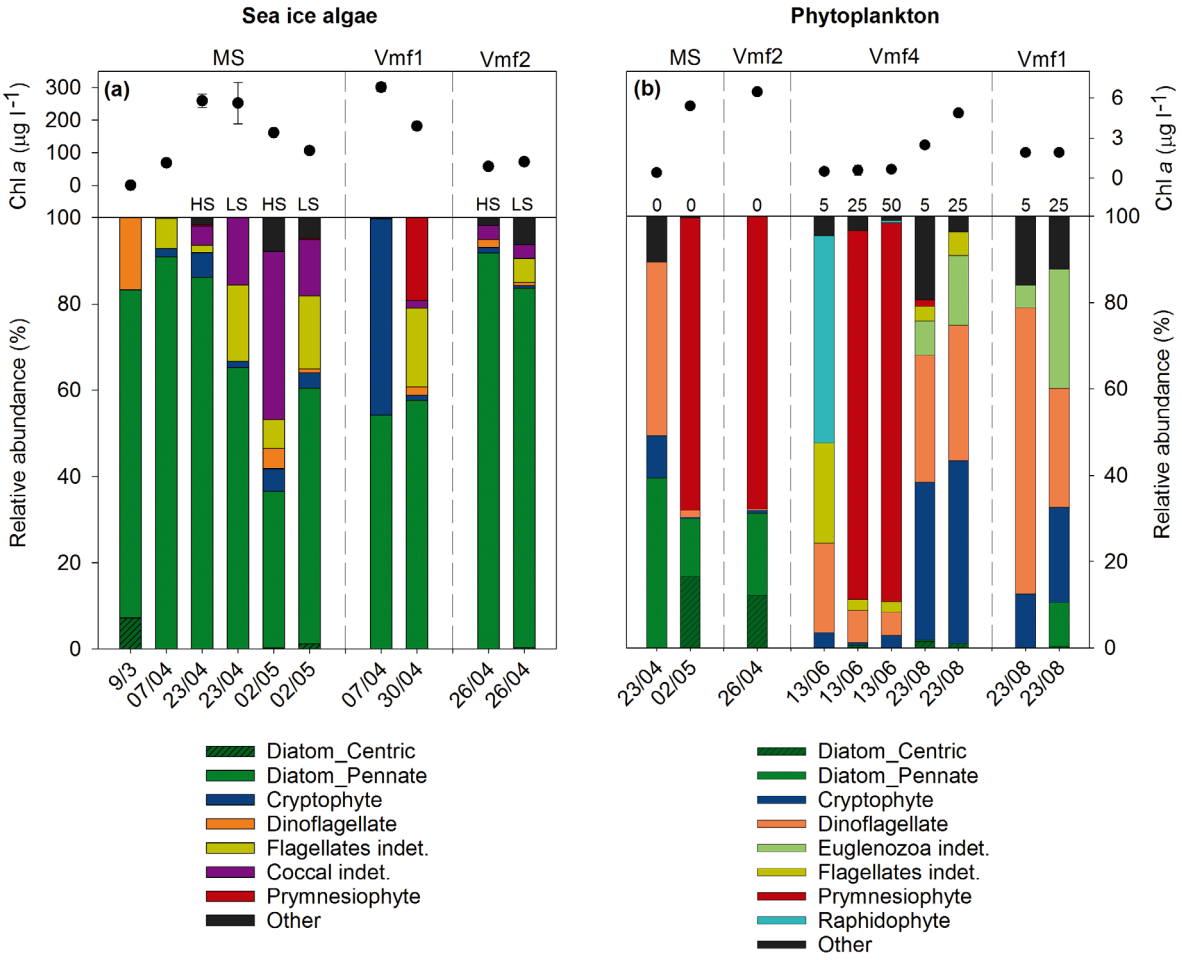

Fig. 3. Abundance (%) of microalgae groups dominating the (a) sea ice algal assemblages and (b) phytoplankton assemblages, as well as chl *a* concentrations from the respective cores and depths. The sea ice algal assemblages are divided by stations (MS, Vmf1 and Vmf2), dates (from 3 March to 2 May 2017) and high (20+ cm) and low (0–5 cm) snow sites (HS and LS, respectively). The phytoplankton assemblages are divided in stations (MS, Vmf2, Vmf4 and Vmf1), dates (from 23 April to 23 August 2017) and water depths (0, 5, 25, 50 m). Phytoplankton samples from Stns MS and Vmf2 were collected under ice, while samples from Vmf4 and Vmf1 were collected from open water. The group 'Other' includes microalgal groups choanoflagellates, chrysophytes, ciliates, dictyochophytes, katablepharids, prasinophytes and Pyramimonadophyceae

phytoplankton community was much more heterogeneous and variable compared to sea ice algae. In April and May, 3 major groups were found to dominate numerically: prymnesiophytes (0–68% of total abundance), diatoms (30–40%) and dinoflagellates (0–40%, Fig. 3b). Particularly abundant taxa were the colony-forming prymnesiophyte *Phaeocystis pouchetii*, the centric diatoms *Chaetoceros* sp. and *Thalassiosira* sp., and the pennate diatom *Fragilariopsis* sp. In June at Stn Vmf4, surface layers (5 m) were largely dominated by 1 known brackish and mixotrophic genus, *Olisthodiscus* (raphidophytes, 48% of total abundance), while the deeper depths (25 and 50 m) were dominated by >80% *P. pouchetii.* In August, the phytoplankton protist assemblage was dominated by heterotrophic and mixotrophic cryptophytes (particularly *Teleaulax* sp.) and dinoflagellates (*Gymnodinium* sp.), in addition to other unidentified flagellates.

3.3. Photophysiological and biochemical responses from field observations

In order to assess ecophysiological responses of natural sea ice algal and phytoplankton assemblages, we followed variable fluorescence characteristics, stoichiometry and pigment composition of the 2 communities, under naturally variable environmental conditions. Some responses were similar between sea ice algae and phytoplankton, such as a positive correlation between the amount of the pho-

toprotective pigments diadinoxanthin and diatoxanthin per chl *a* ([DD+DT]:chl *a* ratios) with irradiance. However, the results also revealed large differences in photosynthetic efficiency and capacity between the 2 algal assemblages, especially when daily average irradiance levels were higher than 8 µmol photons m^{-2} s^{-1}, and NO_3^- levels were depleted (<0.5 µmol l^{-1}).

F_v/F_m, the maximum dark-acclimated PSII quantum yield, of the sea ice algal assemblages ranged from 0.05 to 0.48, and was significantly correlated with both irradiance (p = 0.0006) and NO_3^- (p = 0.0008; Fig. 4a). However, the relation between F_v/F_m and irradiance was not linear. After log-transforming the different variables, we can deduce that for a 10% increase in irradiance, sea ice algal F_v/F_m increased by 3.3% up to daily average values of ~6 µmol photons m^{-2} s^{-1}. When irradiance levels increased >8 µmol photons m^{-2} s^{-1}, sea ice algal F_v/F_m started to decrease by 3.4% for every 10% increase in irradiance (Fig. 4b). The relation between F_v/F_m and NO_3^- levels increased linearly (by 2.9% for every 10% increase in NO_3^-) in sea ice algae (Fig. 4c). Hence, the lowest sea ice algal F_v/F_m values (<0.1) were observed under high irradiance (greater than average daily irradiance of 74 µmol photons m^{-2} s^{-1}, with peak irradiance reaching ~305 µmol photons m^{-2} s^{-1}) and low NO_3^- (<0.5 µmol l^{-1}) levels. F_v/F_m of phytoplankton ranged from 0.06 to 0.55, with the highest values being observed between mid-March and early May (0.32–0.55), when communities were dominated by prymnesiophytes, diatoms and dinoflagellates (Fig. S1). Phytoplankton F_v/F_m was lowest in June and August, when mixotrophic and heterotrophic microalgal groups dominated the assemblages (e.g. raphidophytes and dinoflagellates). By then, nitrate levels were low (<1 µmol l^{-1}), and irradiance was highly variable due to high sediment loads from terrestrial runoff in the innermost station, i.e. either <1 µmol photons m^{-2} s^{-1} (Vmf1) or >50 µmol photons m^{-2} s^{-1} (Vmf4). Phytoplankton F_v/F_m was not significantly correlated with irradiance (Fig. 4e), but a slight, albeit non-significant, positive relationship was observed between F_v/F_m and NO_3^- levels

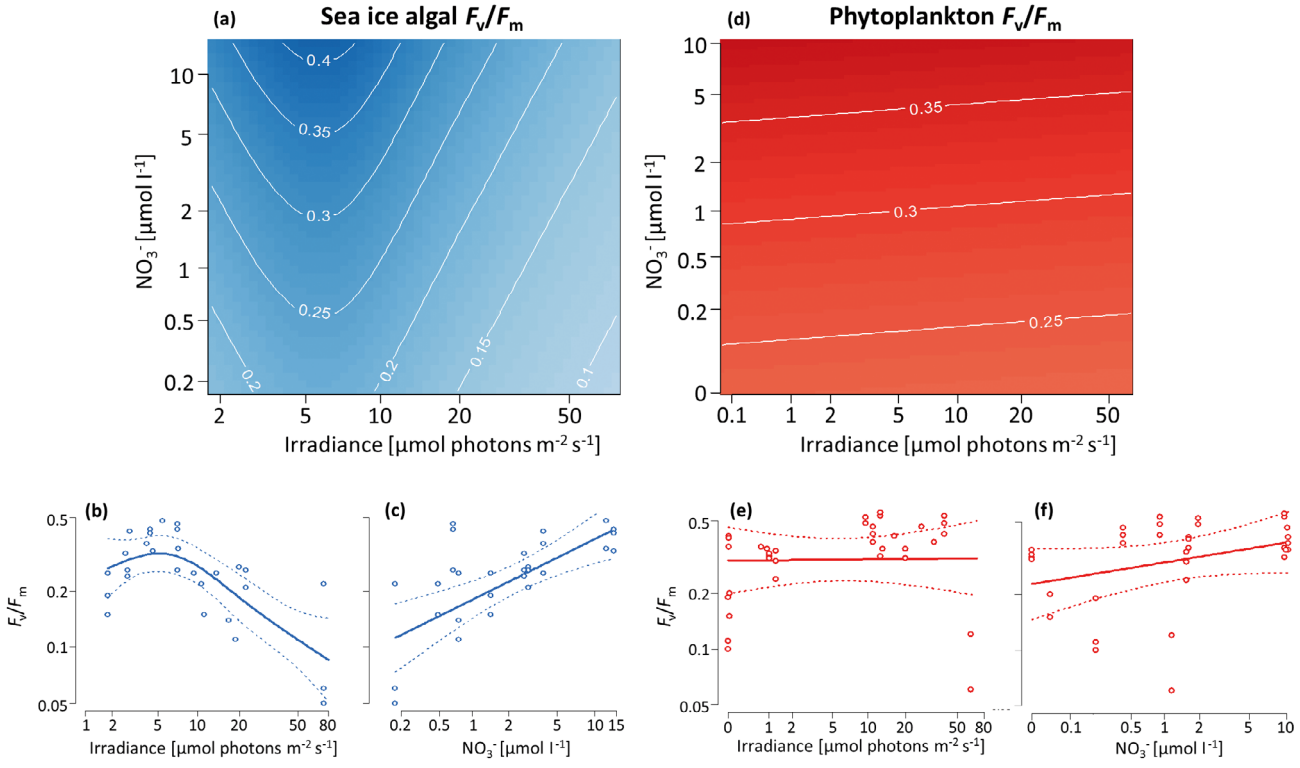

Fig. 4. Contour plots of the generalized additive mixed modeling (GAMM) fitted values, showing modeled changes in the maximum dark-acclimated quantum yield of PSII (F_v/F_m) in response to daily average irradiance and NO_3^- levels in (a) sea ice algae and (d) phytoplankton algal assemblages. The 4 bottom graphs show marginal plots for (b,c) sea ice algae and (e,f) phytoplankton, where changes in F_v/F_m are separated for daily average irradiance (b,e) and NO_3^- levels (c,f). Sea ice algae were collected from areas with varying snow depth (0–27 cm), and phytoplankton were collected from 0, 5, 25 and 50 m depths. All variables are log transformed, and in the lower plots, raw data values are shown with GAMM curve fits expressed as solid lines and confidence intervals expressed as dotted lines

(Fig. 4f). Further analysis revealed that in phytoplankton communities dominated primarily by photosynthetic organisms (i.e. being more similar to the sea ice algal assemblages), F_v/F_m increased slightly with increasing irradiance ($p = 0.003$; data not shown). The absorption cross-section of PSII (σ_{PSII}) did not show any significant trends with irradiance and NO_3^- levels in either sea ice algae or phytoplankton (data not shown), and the averaged values did not differ significantly between the 2 communities (Table 2). Similarly, no apparent trends in τ_{ES} (indicating the kinetics of electron transport on the acceptor side of PSII) with changing irradiance and nutrient regimes were observed in either sea ice algae or phytoplankton. However, the averaged τ_{ES} was almost twice as high in the sea ice algal communities (Student's *t*-test, $t_{52} = 3.2$, $p = 0.003$; Table 2).

Results from FRRf-based FLCs and biochemical analysis revealed substantial differences in the acclimation capacity of sea ice algal and phytoplankton communities. Regarding the light utilization coefficient, sea ice algae showed consistently decreasing αETR, by 3.6% for every 10% increase in irradiance ($p = 0.003$, Fig. 5a). Moreover, in correspondence with αETR, we observed a significant increase of POC:chl *a* content in the sea ice community with increasing irradiance levels ($p < 0.0001$, Fig. 5b), where POC:chl *a* ratios increased by 3.5% for every 10% increase in irradiance. In contrast, αETR and POC:chl *a* varied strongly in the phytoplankton communities, ranging from 0.14 to 0.51 mol e^- m^2 (mol RCII)$^{-1}$ (mol photons)$^{-1}$ and from 11.9 to 1027.6 µg C (µg chl *a*)$^{-1}$, respectively, and the resulting relationship with irradiance was non-significant for both parameters (Fig. 5a,b).

The amount of the photoprotective pigments relative to chl *a* ([DD+DT]:chl *a*) showed an increasing trend with irradiance in both sea ice algal and phytoplankton assemblages (Fig. 5c). In sea ice algae, (DD+DT):chl *a* increased by 1.3% for every 10% increase in irradiance in the low irradiance range between 2 and 10 µmol photons m^{-2} s^{-1}, and thereafter by 7.6% ($p < 0.0001$). In phytoplankton, (DD+DT):chl *a* ratios increased by 2.7% for every 10% increase in irradiance, but were not significantly correlated. With respect to NPQ at a measured light intensity of 300 µmol photons m^{-2} s^{-1} (NPQ_{300}), sea ice algae showed an increasing trend in NPQ_{300} with irradiance (by 4% for every 10% increase in irradiance), but the relationship was not significant (Fig. 5d). In the phytoplankton communities, in contrast, NPQ_{300} decreased significantly with increasing irradiance ($p = 0.02$, Fig. 5d). Due to these 2 distinct responses between the algal assemblages, the average NPQ_{300} was significantly higher in sea ice algae (13 ± 7.2) compared to phytoplankton (4.9 ± 3.2; Student's *t*-test, $t_{52} = 5.3$, $p < 0.0001$, Table 2).

Maximum electron transport rates ($rETR_{max}$) were significantly correlated with irradiance in sea ice algae ($p = 0.04$), although this relationship was not linear; at daily average irradiance levels up to

Table 2. Mean (SD) photosynthetic parameters in sea ice algal and phytoplankton assemblages from field observations (fast repetition rate fluorometry [FRRf]-based parameters only), and from the *in situ* incubation experiment conducted underneath the sea ice (FRRf- and ^{14}C-based parameters). Maximum dark-acclimated PSII quantum yield (F_v/F_m), absorption cross-section of PSII (σ_{PSII} [nm^2 $PSII^{-1}$]), rate of reopening of PSII reaction centers (τ_{ES} [ms]) and non-photochemical quenching (NPQ_{300}) were derived from FRRf variable fluorescence measurements. Fit parameters ($rETR_{max}$, P_{max}, αETR, α and E_kETR and E_k) were derived from either FRRf-based fluorescence light curves or ^{14}C-based photosynthesis vs. irradiance curves. FRRf-derived $rETR_{max}$ [mol e^- (mol RCII)$^{-1}$ s^{-1}] is the light-saturated maximum rate of charge separation in RCII, while the FRRf-derived αETR is the light-dependent increase of charge separation in RCII before saturation (mol e^- m^2 [mol RCII]$^{-1}$ [mol photons]$^{-1}$). ^{14}C-derived P_{max} is the light saturated maximum rate of ^{14}C uptake (µg C [µg chl *a*]$^{-1}$ d^{-1}). ^{14}C-derived α is the initial light-limited slope (µg C [µg chl *a*]$^{-1}$ d^{-1} [µmol photons m^{-2} s^{-1}]$^{-1}$). Both FRRf- and ^{14}C-derived E_k is the photoacclimation index (µmol photons m^{-2} s^{-1}). *Significant difference ($p < 0.05$) between sea ice algae and phytoplankton; na: not available

	Field observations			*In situ* incubation experiment			
	FRRf-based			FRRf-based		^{14}C-based	
	Sea ice algae		Phytoplankton	Sea ice algae	Phytoplankton	Sea ice algae	Phytoplankton
F_v/F_m	0.27 (0.12)	*	0.34 (0.14)	0.37 (0.06)	0.38 (0.05)	na	na
σ_{PSII}	5.1 (1.2)		5.3 (0.9)	5.3 (0.2)	* 5.9 (0.1)	na	na
τ_{ES}	7.6 (4.8)	*	4.7 (1.7)	4.2 (0.4)	3.9 (0.4)	na	na
NPQ_{300}	13.0 (7.2)	*	4.9 (3.2)	2.4 (0.4)	* 1.5 (0.1)	na	na
$rETR_{max}$, P_{max}	31 (23)	*	80 (37)	41 (3)	* 94 (2)	0.18	na
αETR, α	0.16 (0.08)	*	0.36 (0.09)	0.34 (0.03)	0.35 (0.07)	0.004	0.009
E_kETR, E_k	221 (156)		217 (69)	120 (2)	* 274 (44)	43	na

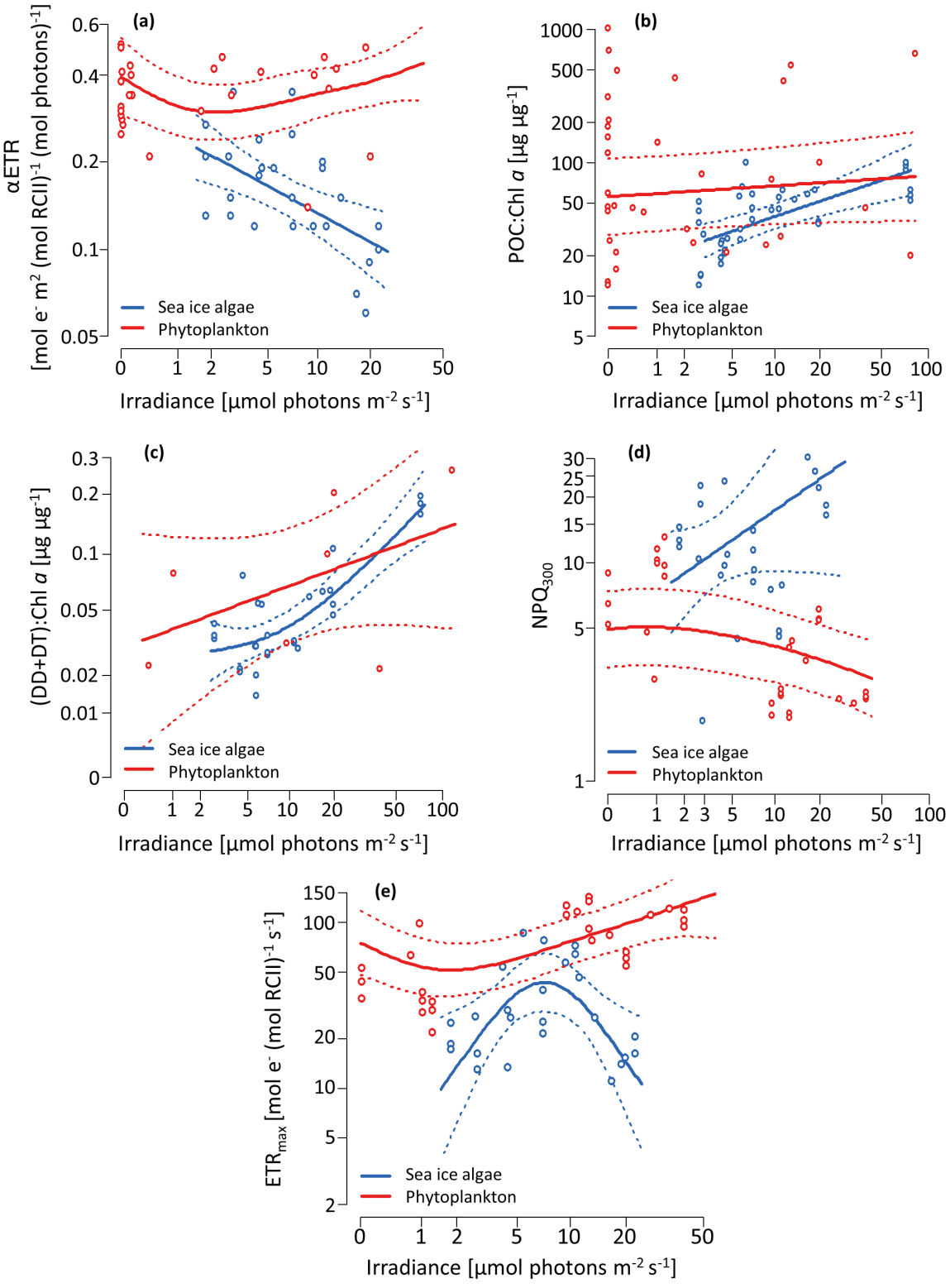

Fig. 5. Changes in (a) light utilization coefficient (αETR), (b) particulate organic carbon (POC) to chl *a* ratios, (c) light protective pigment ratios (diadinoxanthin and diatoxanthin [DD+DT]:chl *a*), (d) non-photochemical quenching at 300 µmol photons m^{-2} s^{-1} (NPQ_{300}) and (e) maximum photosynthetic rate ($rETR_{max}$) in response to daily average irradiance levels in sea ice algae and phytoplankton. Sea ice algae were collected from areas with varying snow depth (0–27 cm), and phytoplankton were collected from 0, 5, 25 and 50 m depths. All variables are log transformed, and raw data values are shown with GAMM curve fits expressed as solid lines and confidence intervals expressed as dotted lines

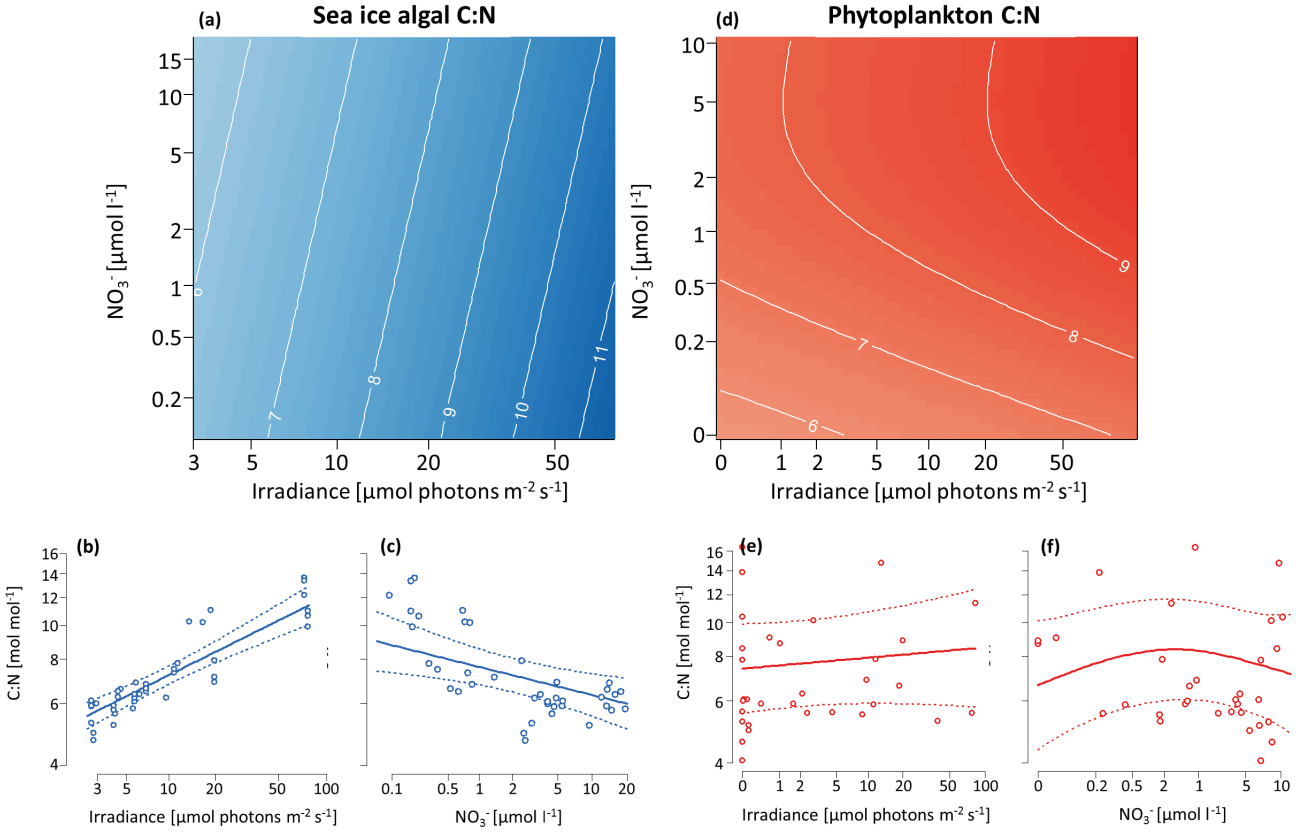

Fig. 6. Contour plots of the GAMM fitted values, showing modeled changes in the particulate organic carbon to particulate organic nitrogen ratios (C:N) in response to daily average irradiance and NO_3^- levels in (a) sea ice algae and (d) phytoplankton algal assemblages. The 4 bottom graphs show marginal plots for (b,c) sea ice algae and (e,f) phytoplankton, where changes in C:N ratios are separated for daily average irradiance (b,e) and NO_3^- levels (c,f). Sea ice algae were collected from areas with varying snow depth (0–27 cm), and phytoplankton were collected from 0, 5, 25 and 50 m depths. All variables are log transformed, and in the lower plots raw data values are shown with GAMM curve fits expressed as solid lines and confidence intervals expressed as dotted lines

approximately 8 µmol photons m^{-2} s^{-1}, sea ice algal $rETR_{max}$ increased on average by 17.2% per 10% increase in light. At higher irradiance, sea ice algal $rETR_{max}$ decreased by 15.3% for every 10% increase in irradiance (Fig. 5e). In comparison, the phytoplankton communities increased their $rETR_{max}$ with increasing irradiance at all levels >2 µmol photons m^{-2} s^{-1} ($p < 0.04$), with values increasing on average by 4.0% for every 10% increase in irradiance (Fig. 5e). Hence, the differences in $rETR_{max}$ between the 2 communities were substantial when irradiance increased >8 µmol photons m^{-2} s^{-1}, resulting in higher averaged $rETR_{max}$ in phytoplankton (80 ± 27 mol e^- [mol RCII]$^{-1}$ s^{-1}) compared to sea ice algae (31 ± 23 mol e^- [mol RCII]$^{-1}$ s^{-1}; Student's *t*-test, t_{52} = 5.4, $p < 0.0001$, Table 2). The relation between $rETR_{max}$ and NO_3^- levels was non-significant in both algal assemblages. Similarly to POC:chl *a* ratios, C:N ratios also showed stronger environmentally driven patterns in sea ice algae compared to phytoplankton. In sea ice algae, C:N ratios increased by 2.2% with a 10% increase in irradiance ($p < 0.0001$, Fig. 6b), while decreasing by 0.80% for every 10% increase in NO_3^- ($p = 0.009$, Fig. 6c). Hence, the responses were strongly negatively correlated between irradiance and NO_3^- levels (correlation = –0.79, Fig. 6a). In phytoplankton assemblages, C:N ratios were highly variable under all irradiance and NO_3^- levels with no significant trends (Fig. 6d–f).

3.4. *In situ* incubation experiment

By measuring variable fluorescence characteristics and ^{14}C-based carbon fixation *in situ* under a range of different irradiances, we were able to assess differences in both the functionality of the photosynthetic apparatus regarding the light-dependent reactions, as well as the ability of sea ice algae and phytoplankton to fix carbon. Additional measurements (e.g.

community composition, *in situ* nutrients and salinity) were not taken on these specific samples on 1 May, but we assume the community and environmental conditions were similar to sampling conducted on 2 May at that station (MS). By then, the majority of the sea ice community (under high snow cover; Fig. 3a) was numerically dominated by coccal unidentified cells ('coccal indet,' 39%) and diatoms (36%; particularly *Fragilariopsis* spp. and *Navicula* spp.). The phytoplankton community was numerically dominated by *Phaeocystis pouchetii* (68%), centric diatoms (17%; particularly *Chaetoceros* spp. and *Thalassiosira* spp.) and pennate diatoms (13%; particularly *Fragilariopsis* spp. and *Nitzschia* spp.; Fig. 3b). Note that phytoplankton samples for the incubation experiment were sampled with a 20 µm phytoplankton net, hence smaller cells were probably largely excluded from the experiment. We therefore expect the communities in the experiment to be dominated by the above-mentioned diatoms as well as *P. pouchetii* (colonies) in case of the phytoplankton community. *In situ* nutrient levels were depleted in both sea ice (NO_3^-: 0.67 µmol l^{-1}, $Si(OH)_4$: 0.31 µmol l^{-1}) and water (NO_3^-: 0.91 µmol l^{-1}, $Si(OH)_4$: 0.34 µmol l^{-1}), and temperatures were reasonably similar between ice and water (−1.7 and −1.6°C, respectively; Table 1). Salinity was lower in sea ice (31.4) than in water (34.6).

Similar to the field observations, this experiment also revealed different ecophysiological characteristics between sea ice algae and phytoplankton. Before incubation under the sea ice, F_v/F_m was within the same range for sea ice algae and phytoplankton, with values of 0.37 ± 0.06 vs. 0.38 ± 0.05, respectively (Table 2). Similarly, no noticeable differences were observed with respect to the rate of reopening of PSII reaction centers (τ_{ES}). The absorption cross section of PSII (σ_{PSII}) was slightly higher in phytoplankton compared to sea ice algal communities (Student's *t*-test, $t_3 = -3.6$, p = 0.04), while NPQ_{300} was significantly lower in the former ($t_3 = 4.6$, p = 0.02, Table 2). Results from the FRRf-based FLCs showed that the $rETR_{max}$ were higher in phytoplankton compared to sea ice algae ($t_3 = -24.5$, $p < 0.001$), while αETR remained similar, resulting in significantly higher FRRf-derived E_kETR in phytoplankton compared to sea ice algae ($t_3 = -4.7$, p = 0.02, Table 2, Fig. 7a). After 24 h incubation underneath the sea ice, phytoplankton showed higher carbon fixation rates at all irradiances compared to the sea ice algae (Fig. 7b). Also, the ^{14}C-derived α in phytoplankton (0.009 µg C [µg chl *a*]$^{-1}$ d^{-1} [µmol photons m^{-2} s^{-1}]$^{-1}$) was higher compared to sea ice algae (0.004 µg C [µg chl *a*]$^{-1}$ d^{-1} [µmol photons m^{-2} s^{-1}]$^{-1}$). Due to lack of light saturation in the phytoplankton assemblage, ^{14}C-based P_{max} and E_k could not be derived from the curve fits. In sea ice algal assemblages, however, light saturation was characterized by a ^{14}C-based E_k of 43 µmol photons m^{-2} s^{-1} and a resulting P_{max} of 0.18 µg C (µg chl *a*)$^{-1}$ d^{-1} (Table 2). Overall, the phytoplankton community showed higher mean carbon fixation

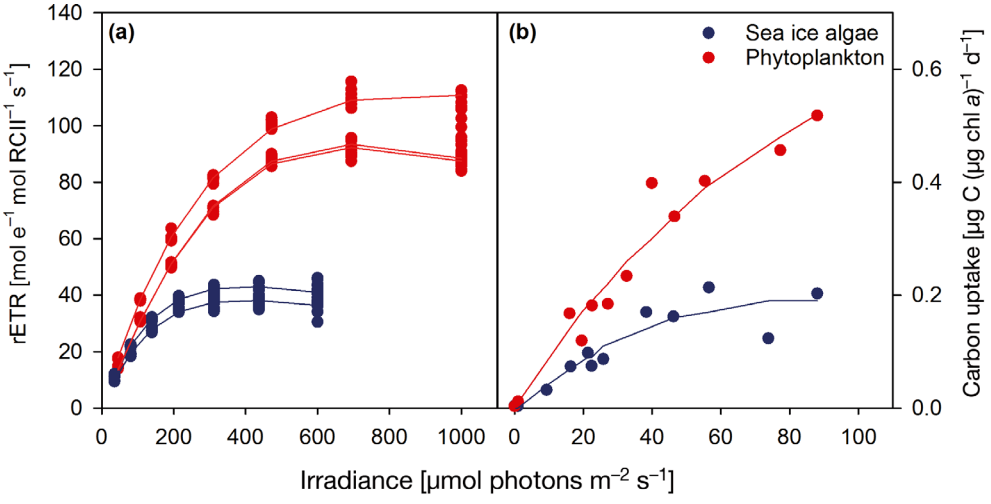

Fig. 7. (a) Fast repetition rate fluorometry (FRRf)-based fluorescence light curves (FLCs) and (b) ^{14}C-based photosynthesis vs. irradiance (*PE*) curves in sea ice algae and phytoplankton from the *in situ* incubation experiment conducted underneath the sea ice in Van Mijenfjorden during the main bloom period in both habitats in 2017. Raw data values of electron transport through photosystem II (rETR; mol e^{-1} [mol RCII]$^{-1}$ s^{-1}) and ^{14}C-fixation (µg C [µg chl *a*]$^{-1}$ d^{-1}) are shown as a function of increasing irradiance and the model fits of Eilers & Peeters (1988) are expressed as lines. Parameters derived from the FRRf-based FLCs and ^{14}C-based *PE* curves are found in Table 2, while the irradiance regimes encountered by the algal assemblages are given in Fig. S2

rates (0.25 ± 0.17 µg C [µg chl a]$^{-1}$ d^{-1}) compared to the sea ice-associated community (0.10 ± 0.07 µg C [µg chl *a*]$^{-1}$ d^{-1}, $t_{22} = -2.8$, p = 0.01).

4. DISCUSSION

In this study, we compared photophysiological and biochemical characteristics of sea ice algal and phytoplankton communities in order to evaluate strategies used by the 2 functionally distinct types of microalgal communities to acclimate to variations in light and nutrients. According to the traditional perception, sea ice algal production peaks earlier in spring, whereas phytoplankton production occurs primarily in open waters subsequent to sea ice retreat (Hill & Cota 2005, Perrette et al. 2011). However, increasing evidence during recent years suggests a more common occurrence of phytoplankton blooms underneath sea ice, which can originate from advected algal blooms in ice-free areas (Johnsen et al. 2018, Ardyna et al. 2020) but have also been found to develop locally (Arrigo et al. 2012, Mundy et al. 2014, Assmy et al. 2017). In the current study, we found that the sea ice algal and phytoplankton blooms in Van Mijenfjorden in 2017 peaked almost simultaneously (Fig. 2c). Despite environmental conditions (i.e. irradiance and nutrient levels) encountered by sea ice algae and phytoplankton being relatively similar in this study, we found distinct differences between the 2 algal communities with respect to their sensitivity to environmental changes.

4.1. Considerable requirement for photoprotection in sea ice algae

Beneath the sea ice in spring when irradiance levels were low (<8 µmol photons m^{-2} s^{-1}) and nutrients were abundant, sea ice algae displayed clear signs of photoacclimation to low light. The observed high F_v/F_m and αETR in combination with generally low NPQ_{300} and (DD+DT):chl *a* ratios (Figs. 4b & 5a,c,d) suggest little requirement of dissipating absorbed energy as heat. This is in line with various studies that have suggested specific adaptions of polar microalgae that enable them to grow under very low irradiances, such as high growth rates, very high cellular chl *a* quota and a low light saturation of photosynthesis (Cota 1985, Kirst & Wiencke 1995, Lacour et al. 2017, Hancke et al. 2018). As daily average irradiances increased towards ~8 µmol photons m^{-2} s^{-1}, significantly decreasing FRRf-derived αETR and increasing POC:chl *a* ratios support that sea ice algae efficiently acclimated to higher irradiances, probably by reducing the quota of photosynthetic pigments (Fig. 5a,b). Furthermore, and in line with previous work, the significant positive relationships between (DD+DT):chl *a* ratios and irradiance in sea ice algae (Fig. 5c) confirms that light transmittance exerts a strong control on carotenoid synthesis even under relatively low irradiance levels (Alou-Font et al. 2013, Galindo et al. 2017). Hence, a rapid decline in light harvesting coupled with increased capacity for photoprotection seems to be the preferred method of balancing energy flow to PSII in sea ice algae with increasing irradiances. Given the strong dominance of diatoms in the sea ice algal assemblages, which are known to efficiently employ such photoprotective mechanisms, the observed responses were as expected (Fig. 3a; von Quillfeldt et al. 2003, Brunet et al. 2011, Alou-Font et al. 2013, Lacour et al. 2020). These light-driven adjustments to the photosynthetic machinery were effective in the low average irradiance range between 0 and 8 µmol photons m^{-2} s^{-1}, and ensured a high level of plasticity in their light-acclimation capabilities. This resulted in elevated maximum dark-acclimated quantum yield of PSII (F_v/F_m) and concurrently allowed for increased maximum electron transport rates through PSII ($rETR_{max}$) towards daily average irradiance levels of ~8 µmol photons m^{-2} s^{-1} (Figs. 4a,b & 5e). When daily irradiance levels increased beyond 8 µmol photons m^{-2} s^{-1}, sea ice algal assemblages clearly invested more energy in photoprotection: (DD+DT):chl *a* ratios increased rapidly with increasing irradiance, and NPQ_{300} approached values >20 (Fig. 5c,d), indicating substantial photoprotective efforts. This increased dissipation of excess excitation energy caused F_v/F_m and $rETR_{max}$ to decrease with increasingly higher irradiances (>8 µmol photons m^{-2} s^{-1}: Figs. 4b & 5e). The observed decrease in $rETR_{max}$ may also indicate photoinactivation of PSII, or that the turnover of proteins associated with photoprotection (such as D1) was not sufficient to sustain high rates of electron transport through PSII (Fig. 5e). Under the highest light (daily average irradiance levels of ~74 µmol photons m^{-2} s^{-1}, with peak irradiance of ~305 µmol photons m^{-2} s^{-1}), F_v/F_m reached extremely low values (0.11 ± 0.09), indicating a strong decline in photosynthetic performance. It is important to note, however, that the highest light often co-occurred with low nutrient levels, resulting in co-occurrence and potential interaction of stressors (as discussed below). We conclude that sea ice algae did not benefit from the increased light availability at average

daily irradiance >8 µmol photons m^{-2} s^{-1} which was frequently observed from 23 April onwards under snow cover <15 cm. This is in line with previous findings of a detrimental effect of high irradiance on sea ice algal communities (Juhl & Krembs 2010, Leu et al. 2010, Alou-Font et al. 2013, Kvernvik et al. 2020).

Changing environmental conditions can cause alterations in cellular C:N ratios of microalgae, deviating from Redfield ratios (Sterner & Elser 2002, Frigstad et al. 2014, Niemi & Michel 2015). Both irradiance and NO_3^- exert strong control on C:N ratios, where values may increase as a result of acclimation to high irradiance (i.e. a relative increase in cellular C quota because excess light energy is drained in C fixation) or nutrient limitation (i.e. a relative decrease in cellular N quota; Demers et al. 1989, Gosselin et al. 1990). In the sea ice algal assemblages, C:N ratios were positively correlated with irradiance and negatively correlated with NO_3^- concentrations, i.e. the highest C:N ratios were observed under high light and low NO_3^- concentrations (Fig. 6a–c). However, since the observations from field data and the *in situ* experiment strongly suggest that sea ice algae were increasingly light stressed at average irradiance >8 µmol photons m^{-2} s^{-1} and thus did not benefit from higher light availability, we hypothesize that the high C:N ratios primarily resulted from increasing nutrient limitation. Synthesis of proteins and pigments required for photoacclimation and photorepair consumes large amounts of nutrients (Eberhard et al. 2008). Congruently, nutrient limitation (in particular NO_3^-) can have a pronounced effect on photosynthetic performance by restricting quantum yield, photochemical efficiency of PSII and growth (Geider et al. 1993, Van De Poll et al. 2005), in addition to increasing susceptibility to photoinhibition (Kiefer 1973, Litchman et al. 2002). The highest F_v/F_m of sea ice algae in this study was observed when light was low (i.e. ~5 µmol photons m^{-2} s^{-1}) and NO_3^- concentrations were high (>10 µmol l^{-1}). The abundant NO_3^- supplies probably supported biosynthesis of photosynthetic pigments (Eberhard et al. 2008, Lewis et al. 2019), and thus enhanced absorption of the limited light available beneath the sea ice. Furthermore, indications of high light stress in sea ice algal assemblages were particularly pronounced when nutrient levels were low, as F_v/F_m decreased to ~0.1 under high light (>50 µmol photons m^{-2} s^{-1}) and low nitrate levels (<0.5 µmol l^{-1}, Fig. 4a). Hence, nutrient limitation probably impeded photoacclimation to these higher irradiance levels during the later stages of the sampling period and contributed to the strongly reduced photosynthetic efficiency in sea ice algal assemblages, hinting towards an interactive effect between irradiance and nutrient levels (Lewis et al. 2019).

4.2. Phytoplankton exhibited a high plasticity towards variable irradiance

Compared to the sea ice algal assemblages, trends in the response to variations in irradiance in phytoplankton were less pronounced in several parameters such as $rETR_{max}$, photoprotective pigment content ([DD+DT]:chl *a*) and NPQ_{300}, and even absent in several measured parameters, e.g. in F_v/F_m, αETR, POC:chl *a* and C:N ratios. As the species composition of the phytoplankton communities were more heterogeneous compared to the sea ice communities (i.e. often mixed between phototrophic and mixotrophic species), and also varied more both in space and time with respect of dominant groups, these lacking trends could in part be explained by community shifts as discussed later in Section 4.4.

It seems that light harvesting of both sea ice algae and phytoplankton was acclimated to the same irradiance range (evidenced by similar averaged E_kETR; Table 2), but that phytoplankton showed overall higher production rates, as both the averaged αETR and rETRmax were higher compared to sea ice algae, and as also indicated by the results of the ^{14}C-based production experiment (Table 2). This difference may be explained by the fact that αETR and $rETR_{max}$ of phytoplankton remained similar over the entire range of irradiance levels that occurred over the study period, which was in strong contrast to the sea ice algae, which substantially lessened electron transport rates in response to increasing irradiance (Fig. 5a,e). Several of the abundant phytoplankton classes recognized during this study possess the diadinoxanthin cycle (i.e. diatoms, dinoflagellates and prymnesiophytes; Lacour et al. 2020). Similar to the sea ice algae, (DD+DT):chl *a* ratios increased with irradiance in phytoplankton; however, this did not translate into increased NPQ_{300}. Consequently, NPQ_{300} was twice as high in sea ice algae compared to phytoplankton at higher irradiance levels (Fig. 5d), confirming that within the same irradiance range, phytoplankton experienced much less photochemical stress and relied less on photoprotection compared to sea ice algae. The absorption cross-section of PSII light-harvesting antenna, σPSII (i.e. energy delivery to PSII), observed in our field samples remained in a similar range in both sea ice algae and

phytoplankton. However, the rate of reopening of PSII reaction centers, τ_{ES}, was significantly lower in the latter (Table 2), indicating that phytoplankton exhibited higher capacity to direct the energy away from PSII (Sakshaug et al. 1997). Substantially more efficient electron drainage in an Arctic pelagic compared to a sea ice diatom exposed to high light have also been found in experiments with unialgal cultures (Kvernvik et al. 2020). This efficient energy drainage into carbon fixation in phytoplankton, which is also seen in the overall higher carbon production in phytoplankton compared to sea ice algae in the *in situ* incubation experiment during the main bloom period (Fig. 7), may help to prevent high-light stress of the photosynthetic apparatus by draining energy into the Calvin Cycle. This possibly explains the lower NPQ_{300} values observed in phytoplankton compared to sea ice algae. We speculate that, while the light levels tested in this study generally did not cause signs of high light stress in phytoplankton, the synthesized photoprotective pigments serve to allow them to deal with further increases in irradiance. The results outlined above clearly indicate that phytoplankton possessed a high plasticity towards increasing irradiance. Based on our data, it seems that phytoplankton achieved successful biomass buildup via acclimatory processes downstream of PSII, while sea ice algae had to rely on photoprotection within the same irradiance levels and thus did not benefit from increased light availability at daily average irradiance >8 µmol photons m^{-2} s^{-1}.

In sea ice algal assemblages, NO_3^- limitation affected photophysiology and contributed to the strongly reduced photosynthetic efficiency in high light/low nutrient environments. In phytoplankton assemblages, however, no notable trends in physiological or biochemical parameters were observed with decreasing NO_3^- concentrations. For example, POC:chl *a* and C:N ratios were very variable (ranging from 12 to 1027 µg C [µg chl *a*]$^{-1}$ and 2–19 mol mol^{-1}, respectively, Figs. 5b & 6e) with no clear trends for either with NO_3^- levels. Phytoplankton assemblages encounter more nutrient resupply on small scales (e.g. from turbulence; Henley et al. 2020) than those growing in the more enclosed sea ice realm, meaning that even though the measured nutrient concentrations were similarly low in ice and open water, nutrient limitation was probably still more pronounced over longer time for the sea ice algal assemblages. Furthermore, POC concentrations are largely decoupled from chl *a* concentrations when heterotrophic/mixotrophic production significantly contributes to organic carbon stocks (Niemi & Michel 2015). Given the heterogeneous phytoplankton community composition, which was also changing dynamically, this could explain the highly variable POC:chl *a* and C:N ratios, and subsequent lacking trends with irradiance and NO_3^- levels in this study (Frigstad et al. 2014). It must be kept in mind that chl *a* is a measure of microalgae, while POC comprises microalgae, hetero- and mixotrophic protists, zooplankton and detritus. Given the very high POC:chl *a* values in some phytoplankton samples, some of this carbon might be associated with species other than phytoplankton and/or detrital carbon, affecting the relationship of both POC:chl *a* and C:N ratios with irradiance and NO_3^- levels. This seems to be true especially in late summer, when mixo- and heterotrophic species and zooplankton biomass typically increase (Willis et al. 2006). As algal-specific POC is difficult to sample and was not measured in this study, this limits the confidence in statements purely based on these ratios. Due to their congruence with other measured parameters, they still serve as a valid proxy during the phototrophically dominated spring period (24 April to 13 June in this study).

4.3. Field observations are validated by the *in situ* incubation experimental data

The field observations indicate that phytoplankton exhibited higher plasticity towards increasing irradiance compared to sea ice algae, which was further corroborated by the *in situ* incubation experiment conducted underneath the sea ice during the main bloom period in both habitats (Fig. 7, Table 2). It should be emphasized that the phytoplankton samples were filtered through a 20 µm net, and as we did not assess taxonomic composition on these specific samples, some caution must be taken in comparing the results between the *in situ* incubation experiment and field measurements. One can, however, expect that the *in situ* taxonomic composition in sea ice and water at Stn MS was similar between 1 and 2 March (Fig. 3), and that the filtering of phytoplankton samples through a 20 µm net definitely had a larger effect and increased the dominance of larger (i.e. diatoms and *Phaeocystis pouchetii* colonies) relative to smaller cells. The photoacclimation index, E_k, is an indication of the irradiance level to which microalgae are acclimated (Sakshaug et al. 1997). In phytoplankton, the FRRf-derived E_kETR during the experiment was higher (274 µmol photons m^{-2} s^{-1}) than in sea ice algae (120 µmol photons m^{-2} s^{-1}; Table 2), and in fact, higher than peak irradiances during the incubation

period (~200 µmol photons m^{-2} s^{-1}; Fig. S2), which could be explained by high plasticity in photosynthetic performance of phytoplankton (Assmy et al. 2017). Furthermore, the ^{14}C-derived *PE* curve (Fig. 7b) revealed that primary production in phytoplankton was light limited at all applied irradiances, which indicates that the ^{14}C-based E_k was higher in phytoplankton compared sea ice algae (43 µmol photons m^{-2} s^{-1}). It should be mentioned that for sea ice algae, the FRRf-derived parameters were measured directly after sampling (in-ice conditions) while the ^{14}C-derived parameters were measured after incubation underneath the sea ice (under-ice conditions). Hence sea ice algae may have acclimated to lower irradiance in the under-ice environment during the incubation, contributing to the 3 times lower ^{14}C-based E_k compared to E_kETR. In view of the high FRRf-derived E_k, the non-saturating ^{14}C-based *PE* curve and the continuously increasing FRRf-derived $rETR_{max}$ from the field observations, we conclude that the phytoplankton tended to be generally light limited throughout this study. Surprisingly, the *in situ* incubation experiment also revealed that phytoplankton were more efficient in utilizing low irradiance for carbon fixation compared to sea ice algae (Fig. 7b), possibly explaining the ability of phytoplankton to generate substantial blooms beneath sea ice (Mundy et al. 2014, Assmy et al. 2017, Ardyna et al. 2020). In addition, while the FRRf-based αETR was similar in sea ice algae and phytoplankton, ^{14}C-based α was twice as high in the latter. Taking into account that sea ice algae may also have acclimated their photosynthetic machinery to lower light during the incubation (and therefore α should increase during the ^{14}C incubation), this might indicate that the energy transfer efficiency from photochemistry to biomass build-up was much higher in phytoplankton compared to sea ice algae under light limitation (Schuback et al. 2016, 2017). It should be noted, however, that no spectral correction was applied, and therefore the incubator light could be different between the 2 methods. While this may affect direct comparison of these 2 measurements and prevents us from calculating conversion factors, it still allows a comparison between samples from the 2 habitats. This suggests that in sea ice algae, a substantial fraction of the photosynthetic energy was used for alternative electron sinks (Schuback et al. 2017), possibly an adaption to deal with the extreme environmental conditions within sea ice. These alternative electron sinks could include nutrient assimilation (Laws 1991), carbon concentrating mechanisms (Giordano et al. 2005), photorespiration (Foyer et al. 2009) and cyclic electron flow through PSI (Miyake & Asada 2003). In summary, natural phytoplankton assemblages exhibited overall higher electron transport and carbon assimilation rates during the incubation underneath the sea ice compared to sea ice algae (Fig. 7). These results are in line with recent experimental findings confirming that a dominant pelagic diatom was better at taking advantage of increasing irradiance than a sea ice diatom (Kvernvik et al. 2020).

4.4. Underlying reasons for the differences between sea ice algae and phytoplankton

As outlined above, the field observations and the *in situ* incubation experiment proved that phytoplankton exhibited higher plasticity towards increasing irradiance, had higher carbon fixation rates (both in low and high light) and were less affected by low NO_3^- levels, compared to sea ice algae which exhibited much lower F_v/F_m under high light and low nitrate levels (Fig. 4a). It is important to consider that temporal developments in the taxonomic composition may contribute to changes in photophysiological parameters (Moore et al. 2006, Suggett et al. 2009). Variations in F_v/F_m and σ_{PSII} that could be attributed to phytoplankton community structure were also seen in the current study (Fig. S1). The sea ice algal assemblages were much more homogeneous (i.e. strongly dominated by pennate diatoms between stations and dates), whereas the phytoplankton communities were more heterogeneous (i.e. mixed and variable dominance of groups) as well as more variable in space and time (Fig. 3b). This could be partially explained by the fact that taxonomic changes within highly diverse phytoplankton communities allow for more efficient selection of genotypes that are better adapted to the prevailing light and nutrient environment (Cullen & MacIntyre 1998, Godhe & Rynearson 2017, Hoppe et al. 2017), while the resupply of new genotypes is restricted in the sea ice realm, potentially causing generally lower diversity. For example, the majority of the phytoplankton communities underneath the sea ice (Stns MS and Vmf2 between 23 April and 2 May) and at deeper depths in June (25 and 50 m on 13 June at Stn Vmf4) was numerically dominated by flagellated cells (mostly *Phaeocystis pouchetii* but also dinoflagellates and cryptophytes; >60%) while diatoms played a smaller role (<40%). This is in accordance with previous studies showing that the genus *Phaeocystis* is particularly well adapted to low-light environments (Sakshaug &

Skjoldal 1989, Moisan & Mitchell 1999, Assmy et al. 2017, Lacour et al. 2017). In June at Stn Vmf4, surface layers were influenced by meltwater runoff, and as a result, the phytoplankton community was numerically dominated (~50%) by the mixotrophic genus *Olisthodiscus*, which typically occurs in brackish waters (Hulburt 1965). In August, when nitrate levels were depleted, the majority of the phytoplankton community consisted of mixotrophic species (especially dinoflagellates and cryptophytes) that have differences in energy acquisition strategies (autotrophy vs. mixotrophy; McKie-Krisberg & Sanders 2014). Changes in photophysiological parameters in phytoplankton communities in this study may therefore be due to both differences in antenna structure among dominant taxa and intracellular pigment packaging which generally increase with cell size (Moore et al. 2006, Suggett et al. 2009). Given the subtle to absent effects of environmental differences on photophysiology and stoichiometry of phytoplankton assemblages, however, variations in inter- and intraspecific composition seem to provide functional redundancy (i.e. multiple species that perform similar roles in an ecosystem) as previously observed for Arctic phytoplankton (Hoppe et al. 2018a, Wolf et al. 2018).

Despite such underlying dynamics, we see clear differences in the acclimation potential of sea ice algal and phytoplankton communities that align well with specific physiology of key species of their habitats (e.g. Kvernvik et al. 2020) as well as the environmental conditions they have adapted to. At first glance, it might seem surprising that phytoplankton exhibited higher carbon fixation rates under low irradiance levels compared to sea ice algae during the main bloom period in both habitats (evident from the *in situ* incubation experiment), especially when sea ice algal production typically peaks in early spring when phytoplankton production is very low. However, large-scale phytoplankton blooms have recently been observed beneath the sea ice (Mundy et al. 2014, Assmy et al. 2017, Ardyna et al. 2020), where irradiance levels are even lower (both due to absorption by sea ice algae and water) than at the ice–water interface. Also, measurable rates of net primary production in Arctic phytoplankton assemblages at light levels as low as 0.5 µmol photons m^{-2} s^{-1} have recently been observed, indicating that phytoplankton communities can retain net productivity under more extreme low light conditions than previously thought (Kvernvik et al. 2018). We thus speculate that because sea ice algae are adapted to extreme conditions of reduced temperature, high salinities and extremely variable nutrient and inorganic carbon levels, they allocate more of the photosynthetic resources (such as ATP and NADPH) for associated cellular processes (e.g. cryoprotection, osmoregulation, nutrient transport, carbon concentrating mechanisms) so that less of the energy is ending up in the Calvin Cycle and subsequent biomass build-up (Behrenfeld et al. 2008). In fact, Goldman et al. (2015) suggested that high levels of cyclic electron flow may be a characteristic of psychrophilic phytoplankton that allows them to account for the associated high ATP demand. Since sea ice algae live in more extreme low temperature regimes than phytoplankton, such alternative pathways for electrons could explain the overall lower carbon fixation rates in the former (Fig. 7b). Furthermore, while sea ice algae showed strong signs of high light stress when average daily irradiance levels increased to >8 µmol photons m^{-2} s^{-1}, the phytoplankton communities were generally light limited within the same irradiance ranges. This could be explained by adaption to strongly contrasting irradiance regimes normally encountered by the 2 algal assemblages. Reported transmittance through ice and snow layers in the Arctic are often very low (Leu et al. 2010, 2015, Campbell et al. 2016, Assmy et al. 2017, Hancke et al. 2018), and since sea ice algae live in a spatially restricted environment that is normally not undergoing rapid changes, they usually experience gradually changing irradiances of low amplitudes. In comparison, vertical mixing of phytoplankton cells within deeply mixed surface layers goes along with strong and rapid fluctuations in irradiance levels (MacIntyre et al. 2000). For example, phytoplankton in open water in Van Mijenfjorden on 21 April 2017 could experience irradiance levels ranging from 0 to 100 µmol photons m^{-2} s^{-1}, due to vertical movement within a mixed layer depth of 20 m (estimated from the thermocline at Stn Vmf1). In comparison, irradiance levels at the ice–water interface the same day ranged between 0.1 and 0.8 µmol photons m^{-2} s^{-1} (Fig. 8). Hence, it is expedient for phytoplankton to evolve pronounced mechanisms for dealing with highly dynamic irradiance conditions (e.g. Behrenfeld et al. 1998, White et al. 2020). This is also true for periodically ice-covered systems such as Arctic fjords, where strong wind events can push the landfast ice out of the fjord over short time spans. This is in line with the fact that Arctic phytoplankton assemblages are also rather resistant to changes in temperature, irradiance and pCO_2, a finding that has been explained by the high environmental variability they have to cope with (Hoppe et al. 2018b).

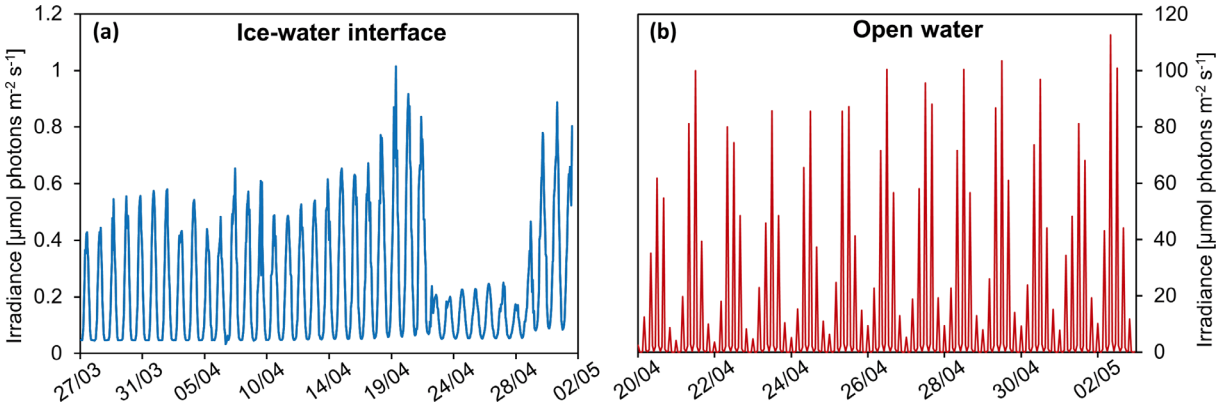

Fig. 8. Temporal changes in the absolute irradiance regimes (a) at the ice–water interface and (b) in open water. Irradiances at the ice–water interface were retrieved from a LI-COR LI-192 Underwater Quantum Sensor measuring photosynthetically active radiation (PAR) every hour between 27 March and 2 May 2017 at Stn MS (see Fig. 1). Daily fluctuations of irradiance regimes in open water were modeled and subsequently corrected for PAR measurements retrieved from the ocean observatory, continuously monitoring PAR every 2 h at 12 m depth at Stn Vmf1 between 20 April and 2 May 2017. Daily integrated surface PAR (measured in May), a K_d of 0.3 m^{-1}, a mixing rate of 0.003 m s^{-1} and 6 mixing cycles d^{-1} were used to model daily irradiance regimes down to 20 m (estimated from thermocline at Stn Vmf1)

It hence seems that both physiological acclimation to variable irradiance and nutrient levels and taxonomic composition must be considered when assessing photosynthetic performance in algal assemblages. The results from this study imply major differences in energy allocation between sea ice algae and phytoplankton when exposed to high light and low nutrients. Sea ice algae seem to allocate more energy into photoprotective mechanisms and alternative energy sinks (e.g. NPQ, photorespiration, Mehler reaction, cyclic electron transport through PSI), that may allow optimization of cellular processes for tolerating extreme environmental conditions but result in lower rates of linear electron transport and carbon assimilation. In phytoplankton, taxonomic and functional changes, as well as high photoacclimative capacity of these taxa together with higher probability of nutrient resupply were probably the underlying reasons for the subtle or absent trends in photophysiology and biochemical responses, but in return ensured high rates of photosynthesis under a wide range of irradiance and NO_3^- levels. It seems that the contrasting environmental conditions in polar seas and sea ice may have led to such specific adaptations and acclimation strategies.

5. CONCLUSION

Knowledge of physiological and biochemical responses of sea ice algae and phytoplankton towards their changing environment is essential to understand how the balance between sea ice-based vs. pelagic primary production will change with respect to timing and quantity in a future Arctic. The results from this study suggest that sea ice algae will be more sensitive than phytoplankton towards the expected environmental changes, in particular increased irradiance. Our findings also clearly highlight the importance of considering interactive effects of environmental variables, as well as the value of comparing functionally distinct communities to gain a mechanistic understanding of response patterns. The contribution of more diverse phytoplankton assemblages, with their high plasticity and potential for functional redundancy, to annual primary production in the Arctic will likely increase, based on the ability of phytoplankton to take advantage of higher irradiances in a habitat that is becoming more prevalent in the future. For sea ice algae, in contrast, we can probably anticipate a decrease in their relative contribution to annual primary production, not only because sea ice cover is generally declining but also because the remaining sea ice is getting thinner and transmits more light, a situation for which our data indicate reduced photosynthetic performance of sea ice algae. These findings may be especially relevant as the importance of ephemeral sea ice (i.e. melting and re-forming) is likely to increase in the future (Onarheim et al. 2018). Hence, organisms inhabiting the sea ice will have to deal with much more dynamic environmental settings, and with ongoing climate change, characteristic sea ice algae species might be outcompeted by less sensitive species, thereby potentially altering the algal colonization of young Arctic sea ice. This could have

important implications for trophic interactions, carbon fluxes and budgets. Hence, an improved and differentiated parameterization of primary production derived from sea ice algae vs. phytoplankton is urgently required in modeling contexts, and needs to include important functional differences of these algal communities as described here.

Acknowledgements. This study was funded by the Norwegian Research Council as part of the project FAABulous: Future Arctic Algae Blooms – and their role in the context of climate change (project nr. 243702), and was partly financed by the Polish Ministry of Science and Higher Education (MNiSW). We thank Laura Wischnewski, Marcel Machnik and Benoit Lebreton for their help with nutrient and organic matter composition sample analyses; Marcel Nicolaus and Martin Schiller for the deployment of SIMBA and the snow buoy; and Dirk Notz and Leif Riemenschneider for the irradiance logger data.

LITERATURE CITED

Alou-Font E, Mundy CJ, Roy S, Gosselin M, Agustí S (2013) Snow cover affects ice algal pigment composition in the coastal Arctic Ocean during spring. Mar Ecol Prog Ser 474:89–104

Ardyna M, Arrigo KR (2020) Phytoplankton dynamics in a changing Arctic Ocean. Nat Clim Change 10:892–903

Ardyna M, Mundy CJ, Mayot N, Matthes LC and others (2020) Under-ice phytoplankton blooms: shedding light on the 'invisible' part of Arctic primary production. Front Mar Sci 7:608032

Arrigo KR, Mock T, Lizotte MP (2010) Primary producers and sea ice. In: Thomas DN, Dieckmann GS (eds) Sea ice, 2nd edn. Wiley-Blackwell, Oxford, p 283–325

Arrigo KR, Perovich DK, Pickart RS, Brown ZW and others (2012) Massive phytoplankton blooms under Arctic sea ice. Science 336:1408

Arrigo KR, Brown ZW, Mills MM (2014) Sea ice algal biomass and physiology in the Amundsen Sea, Antarctica. Elem Sci Anth 2:000028

Assmy P, Fernández-Méndez M, Duarte P, Meyer A and others (2017) Leads in Arctic pack ice enable early phytoplankton blooms below snow-covered sea ice. Sci Rep 7:40850

Aumack C, Juhl A (2015) Light and nutrient effects on the settling characteristics of the sea ice diatom *Nitzschia frigida*. Limnol Oceanogr 60:765–776

Barlow RG, Gosselin M, Legendre L, Therriault JC, Demers S, Mantoura RFC, Llewellyn CA (1988) Photoadaptive strategies in sea-ice microalgae. Mar Ecol Prog Ser 45:145–152

Bates SS, Cota GF (1986) Fluorescence induction and photosynthetic responses of Arctic ice algae to sample treatment and salinity. J Phycol 22:421–429

Behrenfeld MJ, Prasil O, Kolber ZS, Babin M, Falkowski PG (1998) Compensatory changes in photosystem II electron turnover rates protect photosynthesis from photoinhibition. Photosynth Res 58:259–268

Behrenfeld MJ, Halsey KH, Milligan AJ (2008) Evolved physiological responses of phytoplankton to their integrated growth environment. Philos Trans R Soc B 363: 2687–2703

Brunet C, Johnsen G, Lavaud J, Roy S (2011) Pigments and photoacclimation processes. In: Roy S, Llewellyn CA, Egeland ES, Johnsens G (eds) Phytoplankton pigments: characterization, chemotaxonomy and applications in oceanography. Cambridge University Press, Cambridge, p 445–454

Campbell K, Mundy C, Landy J, Delaforge A, Michel C, Rysgaard S (2016) Community dynamics of bottom-ice algae in Dease Strait of the Canadian Arctic. Prog Oceanogr 149:27–39

Carmack E, Wassmann P (2006) Food webs and physical–biological coupling on pan-Arctic shelves: unifying concepts and comprehensive perspectives. Prog Oceanogr 71:446–477

Coello-Camba A, Agustí S, Vaqué D, Holding J, Arrieta JM, Wassmann P, Duarte CM (2015) Experimental assessment of temperature thresholds for Arctic phytoplankton communities. Estuaries Coasts 38:873–885

Cosgrove J, Borowitzka MA (2010) Chlorophyll fluorescence terminology: an introduction. In: Suggett D, Prášil O, Borowitzka M (eds) Chlorophyll *a* fluorescence in aquatic sciences: methods and applications. Developments in applied phycology, Vol 4. Springer, Dordrecht, p 1–17

Cota GF (1985) Photoadaptation of high Arctic ice algae. Nature 315:219–222

Cota GF, Legendre L, Gosselin M, Ingram R (1991) Ecology of bottom ice algae: I. Environmental controls and variability. J Mar Syst 2:257–277

Cox G, Weeks W (1986) Changes in the salinity and porosity of sea-ice samples during shipping and storage. J Glaciol 32:371–375

Cullen JJ, MacIntyre JG (1998) Behavior, physiology and the niche of depth-regulating phytoplankton. NATO Adv Sci I G-Eco 41:559–580

Daase M, Falk-Petersen S, Varpe Ø, Darnis G and others (2013) Timing of reproductive events in the marine copepod *Calanus glacialis*: a pan-Arctic perspective. Can J Fish Aquat Sci 70:871–884

Danielson SL, Eisner L, Ladd C, Mordy C, Sousa L, Weingartner TJ (2017) A comparison between late summer 2012 and 2013 water masses, macronutrients, and phytoplankton standing crops in the northern Bering and Chukchi Seas. Deep Sea Res II 135:7–26

Demers S, Legendre L, Maestrini SY, Rochet M, Ingram RG (1989) Nitrogenous nutrition of sea-ice microalgae. Polar Biol 9:377–383

Eberhard S, Finazzi G, Wollman FA (2008) The dynamics of photosynthesis. Annu Rev Genet 42:463–515

Eilers P, Peeters J (1988) A model for the relationship between light intensity and the rate of photosynthesis in phytoplankton. Ecol Model 42:199–215

Foyer CH, Bloom AJ, Queval G, Noctor G (2009) Photorespiratory metabolism: genes, mutants, energetics, and redox signaling. Annu Rev Plant Biol 60:455–484

Frigstad H, Andersen T, Bellerby RG, Silyakova A, Hessen DO (2014) Variation in the seston C:N ratio of the Arctic Ocean and pan-Arctic shelves. J Mar Syst 129:214–223

Galindo V, Gosselin M, Lavaud J, Mundy CJ and others (2017) Pigment composition and photoprotection of Arctic sea ice algae during spring. Mar Ecol Prog Ser 585:49–69

Garrison DL, Buck KR (1986) Organism losses during ice melting: a serious bias in sea ice community studies. Polar Biol 6:237–239

Geider RJ, La Roche J, Greene RM, Olaizola M (1993) Response of the photosynthetic apparatus of *Phaeodactylum tricornotum* (Bacillariophyceae) to nitrate, phosphate, or iron starvation. J Phycol 29:755–766

Giordano M, Beardall J, Raven JA (2005) CO_2 concentrating mechanisms in algae: mechanisms, environmental modulation, and evolution. Annu Rev Plant Biol 56:99–131

Godhe A, Rynearson T (2017) The role of intraspecific variation in the ecological and evolutionary success of diatoms in changing environments. Philos Trans R Soc Lond B 372:20160399

Goldman JAL, Kranz SA, Young JN, Tortell PD, Stanly RHR, Bender ML, Morel FMM (2015) Gross and net production during the spring bloom along the Western Antarctic Peninsula. New Phytol 205:182–191

Gosselin M, Legendre L, Therriault JC, Demers SJ (1990) Light and nutrient limitation of sea-ice microalgae (Hudson Bay, Canadian Arctic). J Phycol 26:220–232

Gosselin M, Levasseur M, Wheeler PA, Horner RA, Booth BC (1997) New measurements of phytoplankton and ice algal production in the Arctic Ocean. Deep Sea Res II 44:1623–1644

Guillard RR, Ryther JH (1962) Studies of marine planktonic diatoms: I. *Cyclotella nana* Hustedt, and *Detonula confervacea* (Cleve) Gran. Can J Microbiol 8:229–239

Hancke K, Lund-Hansen LC, Lamare ML, Højlund Pedersen S, King MD, Andersen P, Sorrell BK (2018) Extreme low light requirement for algae growth underneath sea ice: a case study from Station Nord, NE Greenland. J Geophys Res Oceans 123:985–1000

Hansell DA, Whitledge TE, Goering JJ (1993) Patterns of nitrate utilization and new production over the Bering–Chukchi shelf. Cont Shelf Res 13:601–627

Hegseth EN, Sundfjord A (2008) Intrusion and blooming of Atlantic phytoplankton species in the high Arctic. J Mar Syst 74:108–119

Henley SF, Porter M, Hobbs L, Braun J and others (2020) Nitrate supply and uptake in the Atlantic Arctic sea ice zone: seasonal cycle, mechanisms and drivers. Philos Trans R Soc A 378:20190361

Hill V, Cota G (2005) Spatial patterns of primary production on the shelf, slope and basin of the Western Arctic in 2002. Deep Sea Res II 52:3344–3354

Hill VJ, Light B, Steele M, Zimmerman RC (2018) Light availability and phytoplankton growth beneath Arctic sea ice: integrating observations and modeling. J Geophys Res Oceans 123:3651–3667

Holm-Hansen O, Riemann B (1978) Chlorophyll *a* determination: improvements in methodology. Oikos 30:438–447

Hoppe CJM, Holtz LM, Trimborn S, Rost B (2015) Ocean acidification decreases the light-use efficiency in an Antarctic diatom under dynamic but not constant light. New Phytol 207:159–171

Hoppe CJM, Schuback N, Semeniuk D, Maldonado MT, Rost B (2017) Functional redundancy mediates phytoplankton resilience to ocean acidification and increased irradiances. Front Mar Sci 4:229

Hoppe CJM, Schuback N, Semeniuk D, Giesbrecht K and others (2018a) Resistance of Arctic phytoplankton to ocean acidification and enhanced irradiance. Polar Biol 41:399–413

Hoppe CJM, Wolf KK, Schuback N, Tortell PD, Rost B (2018b) Compensation of ocean acidification effects in Arctic phytoplankton assemblages. Nat Clim Change 8:529–533

Hoppe CJM, Wischnewski L, Leu E, Brown T and others (2020) Inorganic nutrients measured on water bottle samples from CTD water-sampler system and ice cores during FAABulous project period (2015–2018). Alfred Wegener Institute, Helmholtz Centre for Polar and Marine Research, Bremerhaven. PANGAEA. https://doi.org/10.1594/PANGAEA.925007

Høyland KV (2009) Ice thickness, growth and salinity in Van Mijenfjorden, Svalbard, Norway. Polar Res 28:339–352

Hulburt EM (1965) Flagellates from brackish waters in the vicinity of Woods Hole, Massachusetts. J Phycol 1:87–94

Huntington HP, Danielson SL, Wiese FK, Baker M and others (2020) Evidence suggests potential transformation of the Pacific Arctic ecosystem is underway. Nat Clim Change 10:342–348

Johnsen G, Norli M, Moline M, Robbins I and others (2018) The advective origin of an under-ice spring bloom in the Arctic Ocean using multiple observational platforms. Polar Biol 41:1197–1216

Juhl AR, Krembs C (2010) Effects of snow removal and algal photoacclimation on growth and export of ice algae. Polar Biol 33:1057–1065

Kangas T (2000) Thermohaline sesongvariasjoner i Van Mijenfjorden. MSc thesis, University of Bergen

Kiefer D (1973) Chlorophyll *a* fluorescence in marine centric diatoms: responses of chloroplasts to light and nutrient stress. Mar Biol 23:39–46

Kirst GO, Wiencke C (1995) Ecophysiology of polar algae. J Phycol 31:181–199

Krause G, Weis E (1991) Chlorophyll fluorescence and photosynthesis: the basics. Annu Rev Plant Biol 42:313–349

Kulk G, van de Poll WH, Buma AGJ (2018) Photophysiology of nitrate limited phytoplankton communities in Kongsfjorden, Spitsbergen. Limnol Oceanogr 63:2606–2617

Kvernvik AC, Hoppe CJM, Lawrenz E, Prášil O, Greenacre M, Wiktor JM, Leu E (2018) Fast reactivation of photosynthesis in arctic phytoplankton during the polar night. J Phycol 54:461–470

Kvernvik AC, Rokitta SD, Leu E, Harms L, Gabrielsen TM, Rost B, Hoppe CJM (2020) Higher sensitivity towards light stress and ocean acidification in an Arctic sea-ice-associated diatom compared to a pelagic diatom. New Phytol 226:1708–1724

Kwok R, Cunningham G, Wensnahan M, Rigor I, Zwally H, Yi D (2009) Thinning and volume loss of the Arctic Ocean sea ice cover: 2003–2008. J Geophys Res Oceans 114:C07005

Lacour T, Larivière J, Babin M (2017) Growth, chl *a* content, photosynthesis, and elemental composition in polar and temperate microalgae. Limnol Oceanogr 62:43–58

Lacour T, Babin M, Lavaud J (2020) Diversity in xanthophyll cycle pigments content and related nonphotochemical quenching (NPQ) among microalgae: implications for growth strategy and ecology. J Phycol 56:245–263

Laws EA (1991) Photosynthetic quotients, new production and net community production in the open ocean. Deep Sea Res A Oceanogr Res Pap 38:143–167

Legendre L, Ackley SF, Dieckmann GS, Gulliksen B and others (1992) Ecology of sea ice biota. 2. Global significance. Polar Biol 12:429–444

Leppäranta M, Manninen T (1988) The brine and gas content of sea ice with attention to low salinities and high temperatures. Internal Rep 88-2. Finnish Institute of Marine Research, Helsinki

Leu E, Wängberg SÅ, Wulff A, Falk-Petersen S, Ørbæk JB,

Hessen DO (2006) Effects of changes in ambient PAR and UV radiation on the nutritional quality of an Arctic diatom (*Thalassiosira antarctica* var. *borealis*). J Exp Mar Biol Ecol 337:65–81

Leu E, Wiktor J, Søreide JE, Berge J, Falk-Petersen S (2010) Increased irradiance reduces food quality of sea ice algae. Mar Ecol Prog Ser 411:49–60

Leu E, Mundy CJ, Assmy P, Campbell K and others (2015) Arctic spring awakening—steering principles behind the phenology of vernal ice algal blooms. Prog Oceanogr 139:151–170

Leu E, Schiller M, Nicolaus M (2018) Snow height on sea ice and sea ice drift from autonomous measurements from buoy 2017S43, deployed during FAABulous 2017. Alfred Wegener Institute, Helmholtz Centre for Polar and Marine Research, Bremerhaven. PANGAEA. https://doi.org/10.1594/PANGAEA.887811

Leu E, Brown TA, Graeve M, Wiktor J and others (2020) Spatial and temporal variability of ice algal trophic markers—with recommendations about their application. J Mar Sci Eng 8:676

Lewis KM, Arntsen AE, Coupel P, Joy-Warren H and others (2019) Photoacclimation of Arctic Ocean phytoplankton to shifting light and nutrient limitation. Limnol Oceanogr 64:284–301

Litchman E, Klausmeier CA (2008) Trait-based community ecology of phytoplankton. Annu Rev Ecol Evol Syst 39:615–639

Litchman E, Neale PJ, Banaszak AT (2002) Increased sensitivity to ultraviolet radiation in nitrogen-limited dinoflagellates: photoprotection and repair. Limnol Oceanogr 47:86–94

Loose B, Miller LA, Elliott S, Papakyriakou T (2011) Sea ice biogeochemistry and material transport across the frozen interface. Oceanography 24:202–218

MacIntyre HL, Kana TM, Geider RJ (2000) The effect of water motion on short-term rates of photosynthesis by marine phytoplankton. Trends Plant Sci 5:12–17

Marks AA, King MD (2014) The effect of snow/sea ice type on the response of albedo and light penetration depth (*e*-folding depth) to increasing black carbon. Cryosphere 8:1625–1638

McKie-Krisberg ZM, Sanders RW (2014) Phagotrophy by the picoeukaryotic green alga *Micromonas*: implications for Arctic Oceans. ISME J 8:1953–1961

McMinn A, Müller MN, Martin A, Ryan KG (2014) The response of Antarctic sea ice algae to changes in pH and CO_2. PLOS ONE 9:e86984

Miyake C, Asada K (2003) The water–water cycle in algae. In: Larkum AWD, Douglas SE, Raven JA (eds) Photosynthesis in algae. Advances in photosynthesis and respiration, Vol 14. Springer, Dordrecht, p 183–204

Moisan TA, Mitchell BG (1999) Photophysiological acclimation of *Phaeocystis antarctica* Karsten under light limitation. Limnol Oceanogr 44:247–258

Moore CM, Suggett DJ, Hickman AE, Kim YN and others (2006) Phytoplankton photoacclimation and photoadaptation in response to environmental gradients in a shelf sea. Limnol Oceanogr 51:936–949

Mundy CJ, Barber D, Michel C (2005) Variability of snow and ice thermal, physical and optical properties pertinent to sea ice algae biomass during spring. J Mar Syst 58:107–120

Mundy CJ, Gosselin M, Gratton Y, Brown K and others (2014) Role of environmental factors on phytoplankton bloom initiation under landfast sea ice in Resolute Passage, Canada. Mar Ecol Prog Ser 497:39–49

Nicolaus M, Katlein C, Maslanik J, Hendricks S (2012) Changes in Arctic sea ice result in increasing light transmittance and absorption. Geophys Res Lett 39:L24501

Niemi A, Michel C (2015) Temporal and spatial variability in sea-ice carbon:nitrogen ratios on Canadian Arctic shelves. Elem Sci Anth 3:000078 Doi: 10.12952/journal.elementa.000078

Nöthig EM, Bracher A, Engel A, Metfies K and others (2015) Summertime plankton ecology in Fram Strait—a compilation of long-and short-term observations. Polar Res 34:23349

Onarheim IH, Eldevik T, Smedsrud LH, Stroeve JC (2018) Seasonal and regional manifestation of Arctic sea ice loss. J Clim 31:4917–4932

Oxborough K (2012) FastPro8 GUI and FRRf3 systems documentation. Chelsea Technologies Group, West Molesey

Perrette M, Yool A, Quartly G, Popova E (2011) Near-ubiquity of ice-edge blooms in the Arctic. Biogeosciences 8:515–524

Peterson BJ, Holmes RM, McClelland JW, Vörösmarty CJ and others (2002) Increasing river discharge to the Arctic Ocean. Science 298:2171–2173

Poulin M, Daugbjerg N, Gradinger R, Ilyash L, Ratkova T, von Quillfeldt C (2011) The pan-Arctic biodiversity of marine pelagic and sea-ice unicellular eukaryotes: a first-attempt assessment. Mar Biodivers 41:13–28

R Core Team (2017) R: a language and environment for statistical computing. R Foundation for Statistical Computing, Vienna

Rat'kova TN, Wassmann P (2002) Seasonal variation and spatial distribution of phyto- and protozooplankton in the central Barents Sea. J Mar Syst 38:47–75

Rodriguez F, Chauton M, Johnsen G, Andresen K, Olsen L, Zapata M (2006) Photoacclimation in phytoplankton: implications for biomass estimates, pigment functionality and chemotaxonomy. Mar Biol 148:963–971

Rousseau V, Mathot S, Lancelot C (1990) Calculating carbon biomass of *Phaeocystis* sp. from microscopic observations. Mar Biol 107:305–314

Runge JA, Therriault JC, Legendre L, Ingram RG, Demers S (1991) Coupling between ice microalgal productivity and the pelagic, metazoan food web in southeastern Hudson Bay: a synthesis of results. Polar Res 10:325–338

Sakshaug E (2004) Primary and secondary production in the Arctic seas. In: Stein R, MacDonald RW (eds) The organic carbon cycle in the Arctic Ocean. Springer, Berlin, p 57–81

Sakshaug E, Skjoldal HR (1989) Life at the ice edge. Ambio 18:60–67

Sakshaug E, Bricaud A, Dandonneau Y, Falkowski PG and others (1997) Parameters of photosynthesis: definitions, theory and interpretation of results. J Plankton Res 19:1637–1670

Schuback N, Flecken M, Maldonado MT, Tortell PD (2016) Diurnal variation in the coupling of photosynthetic electron transport and carbon fixation in iron-limited phytoplankton in the NE subarctic Pacific. Biogeosciences 13:1019–1035

Schuback N, Hoppe CJM, Tremblay JÉ, Maldonado MT, Tortell PD (2017) Primary productivity and the coupling of photosynthetic electron transport and carbon fixation in the Arctic Ocean. Limnol Oceanogr 62:898–921

Screen JA, Simmonds I (2012) Declining summer snowfall in the Arctic: causes, impacts and feedbacks. Clim Dyn 38:2243–2256

Screen JA, Simmonds I, Keay K (2011) Dramatic interannual changes of perennial Arctic sea ice linked to abnormal summer storm activity. J Geophys Res 116: D151050

Søreide JE, Hop H, Carroll ML, Falk-Petersen S, Hegseth EN (2006) Seasonal food web structures and sympagic–pelagic coupling in the European Arctic revealed by stable isotopes and a two-source food web model. Prog Oceanogr 71:59–87

Søreide JE, Leu E, Berge J, Graeve M, Falk-Petersen S (2010) Timing of blooms, algal food quality and *Calanus glacialis* reproduction and growth in a changing Arctic. Glob Change Biol 16:3154–3163

Sterner R, Elser JJ (2002) Ecological stoichiometry: the biology of elements from molecules to the biosphere. Princeton University Press, Oxford

Strom SL, Olson MB, Macri EL, Mordy CW (2006) Cross-shelf gradients in phytoplankton community structure, nutrient utilization, and growth rate in the coastal Gulf of Alaska. Mar Ecol Prog Ser 328:75–92

Suggett DJ, Moore CM, Hickman AE, Geider RJ (2009) Interpretation of fast repetition rate (FRR) fluorescence: signatures of phytoplankton community structure versus physiological state. Mar Ecol Prog Ser 376:1–19

Swinehart DJ (1962) The Beer-Lambert law. J Chem Educ 39:333–335

Torstensson A, Dinasquet J, Chierici M, Fransson A, Riemann L, Wulff A (2015) Physicochemical control of bacterial and protist community composition and diversity in Antarctic sea ice. Environ Microbiol 17:3869–3881

Tremblay JÉ, Gagnon J (2009) The effects of irradiance and nutrient supply on the productivity of Arctic waters: a perspective on climate change. In: Nihoul JCJ, Kostianoy AG (eds) Influence of climate change on the changing Arctic and Sub-Arctic conditions. NATO Sci Peace Sec C. Springer, Dordrecht, p 73–93

Utermöhl H (1958) Zur Vervollkommnung der quantitativen Phytoplankton-Methodik. Mitt Int Ver Theor Angew Limnol 9:1–38

Van De Poll WH, Van Leeuwe MA, Roggeveld J, Buma AGJ (2005) Nutrient limitation and high irradiance acclimation reduce PAR and UV-induced viability loss in the Antarctic diatom *Chaetoceros brevis* (Bacillariophyceae). J Phycol 41:840–850

Van De Poll WH, Maat DS, Fischer P, Rozema PD and others (2016) Atlantic advection driven changes in glacial meltwater: effects on phytoplankton chlorophyll *a* and taxonomic composition in Kongsfjorden, Spitsbergen. Front Mar Sci 3:200

Varela DE, Crawford DW, Wrohan IA, Wyatt SN, Carmack EC (2013) Pelagic primary productivity and upper ocean nutrient dynamics across Subarctic and Arctic Seas. J Geophys Res Oceans 118:7132–7152

von Quillfeldt CH, Ambrose WG, Clough LM (2003) High number of diatom species in first-year ice from the Chukchi Sea. Polar Biol 26:806–818

Weeks WF, Ackley SF (1986) The growth, structure, and properties of sea ice. In: Untersteiner N (ed) The geophysics of sea ice. Springer, Boston, MA, p 9–164

White E, Hoppe CJM, Rost B (2020) The Arctic picoeukaryote *Micromonas pusilla* benefits from ocean acidification under constant and dynamic light. Biogeosciences 17: 635–647

Willis K, Cottier F, Kwasniewski S, Wold A, Falk-Petersen S (2006) The influence of advection on zooplankton community composition in an Arctic fjord (Kongsfjorden, Svalbard). J Mar Syst 61:39–54

Wolf KKE, Hoppe CJM, Rost B (2018) Resilience by diversity: large intraspecific differences in climate change responses of an Arctic diatom. Limnol Oceanogr 63: 397–411

Wood S (2017) Package 'mgcv'. R package version 1.7-29. https://cran.r-project.org/web/packages/mgcv/index.html

Editorial responsibility: Steven Lohrenz, New Bedford, Massachusetts, USA
Reviewed by: 3 anonymous referees

Submitted: July 16, 2020
Accepted: February 22, 2021
Proofs received from author(s): May 6, 2021